Department of AERONAUTICS and ASTRONAUTICS
STANFORD UNIVERSITY

PETER E. OETTINGER

A UNIFIED TREATMENT OF THE RELAXATION PHENOMENON IN RADIATING ARGON PLASMA FLOWS BEHIND INCIDENT AND BOW SHOCK WAVES

SUBMITTED BY B. BERSHADER

JULY 1966

Jointly supported by the National Aeronautics and Space Administration, Grant NGR 05-020-091 and by a Ford Foundation Plasma Grant

SUDAAR NO. 285*

*also issued as SU-IPR Report No. 86 of the Institute for Plasma Research, Stanford University

Department of Aeronautics and Astronautics
Stanford University
Stanford, California

A UNIFIED TREATMENT OF THE RELAXATION PHENOMENON IN RADIATING ARGON PLASMA FLOWS BEHIND INCIDENT AND BOW SHOCK WAVES

by

Peter E. Oettinger

SUDAAR 285
July 1966

Submitted by D. Bershader

Jointly supported by the
National Aeronautics and Space Administration,
Grant NGR 05-020-091 and by a
Ford Foundation Plasma Grant

This Report was also Issued as Report No. 86 of
the Institute for Plasma Research, Stanford University

ABSTRACT

The electronic relaxation of a shock heated, nonequilibrium argon plasma flow is treated by means of a combined theoretical and experimental investigation. A physical model of the flow is postulated which includes the microscopic collisional and radiative processes. When coupled with the macroscopic conservation laws, this leads to a rigorous formulation of the equations governing the relaxing flow. A resultant numerical solution for the flow behind a strong incident shock front propagating into argon gas is compared to time-resolved interferograms. Good agreement is obtained between theory and experiment for incident shock Mach numbers of 11 to 18 propagating into argon at pressures of 3 to 5mm Hg. The experimental investigation is extended into the argon shock layer preceding a cylinder-plate. An attempt is made to use the formulated equations to predict conditions along the stagnation streamline, when the flow can either be considered one-dimensional or at constant density across most of the shock layer. Comparison of the experimental and theoretical results show that neither one of these postulated flows actually exists.

ACKNOWLEDGMENTS

The author is indebted to Dr. Daniel Bershader for his supervision and guidance throughout the theoretical and experimental phases of this program, Dr. Kenneth P. Horn for his stimulating interest and helpful advice in the theoretical analysis and his aid with the experimentation, Dr. Howard Wong for his consultations concerning experimental details, Mr. Roger Turcotte for his excellent help in designing and machining the equipment, and Miss Rosemarie Stampfel for typing the manuscript. Personal gratitude is extended also to the Lockheed Missiles and Space Company for allowing use of some of their equipment, and to the Advanced Research Projects Agency, the Ford Foundation, and the National Aeronautics and Space Administration for financing this study.

TABLE OF CONTENTS

TABLE OF CONTENTS CONT.

TABLE OF CONTENTS CONT.

LIST OF FIGURES

LIST OF FIGURES CONT.

LIST OF FIGURES CONT.

NOMENCLATURE

$A(p)$ = argon atom in energy level p

$\bar{A}(p,q)$ = Einstein coefficient for spontaneous transitions from energy level p to q

a = speed of sound; a_e at thermal equilibrium

$\bar{B}(p,q)$ = Einstein coefficient for stimulated transitions from energy level p to q

b_0 = minimum elastic impact distance between an electron and an ion

c = velocity of light in vacuum

d_D = Debye length

$E_{p,q}$ = differential energy between levels p and q

e = elementary charge

e_e = thermal energy of free electrons per unit mass of gas

e_g = internal energy of the gas per unit mass of gas

$f(\epsilon)$ = distribution function for the free electrons

$f_{p,q}$ = oscillator strength for an electronic transition between levels p and q

$g(p)$ = statistical weight of the energy level p

h = Planck constant

h_e = enthalpy of the free electrons per unit mass of gas

h_g = enthalpy of the gas per unit mass of gas

I = ionization potential

I_ν = specific intensity

j = total angular momentum quantum number; J_c refers to the core

j_ν = mass emission coefficient

$K(p,q)$ = rate coefficient for atomic transition from level p to q

$\bar{K}$ = absorptivity

k = Boltzmann constant

k_ν = volume absorption coefficient

L = optical path length

M = Mach number

m_A = mass of the argon atom

m_e = mass of the electron

N = refractive index

N_c = complex refractive index

n = number density

n_A = number density of atoms

n_e = number density of electrons

n_i = number density of ions; for single ionization $n_i = n_e$

$n(p)$ = number density of atoms in energy level p

p = pressure of the gas

p_e = pressure of the free electrons

$Q(T_e)$ = partition function for the atom

$Q_i(T_e)$ = partition function for the ion

q_B = rate of radiant energy loss per unit volume, due to bound-bound transitions

q_c = rate of radiant energy loss per unit volume, due to bremsstrahlung and free-bound transitions

q_R = total rate of radiant energy loss per unit volume

R = gas constant for argon

r = range of interaction between atoms

$S_{1,2}$ = fringe shift between locations 1 and 2

T = temperature

T_A = heavy particle translational temperature

T_e = electron temperature

t = time

u = velocity of the gas

W = electronic energy of the excited atoms per unit mass of gas

x = coordinate along direction of shock propagation

Z_{eff} = effective nuclear charge (in ratio to the charge of a proton)

α = degree of ionization; for a partially singly ionized gas, $\alpha = n_e m_A/\rho$

$\beta(p,z)$ = rate coefficient for photoionization from energy level p

γ = specific heat ratio; γ_e at thermal equilibrium

ϵ = relative energy of the colliding particles

ϵ_c = complex dielectric constant

κ_ν = mass absorption coefficient

λ = wavelength

$\nu_{p,q}$ = frequency corresponding to the transition between energy levels p and q

ν_c = cutoff frequency

ρ = density of the gas

$\rho_R(\nu_{p,q})$ = radiation density for transitions between energy levels p and q

$\sigma_{A\text{-}A}(\epsilon)$ = atom-atom ionization cross-section

$\sigma_{e\text{-}A}(\epsilon)$ = electron-atom ionization cross-section

$\sigma'_{e\text{-}A}(T_e)$ = electron-atom average elastic cross-section

τ_ν = optical depth

φ = rate of thermal energy gain by the free electrons per unit volume

Ψ_c = complex polarizability (Ψ = real part; $i\Psi'$ = imaginary part)

ω = impressed optical frequency ($\omega \equiv 2\pi\nu$)

ω_p = plasma frequency

CHAPTER 1

INTRODUCTION

1.1 INTRODUCTORY COMMENTS

In accordance with a growing interest during the past few years in the determination of atomic reactions within high temperature flows, a number of investigators have conducted theoretical and experimental studies of the behavior of a gaseous flow suddenly subjected to a radical pulse change in temperature and pressure. They observed that the gas particles, unable to adjust instantaneously to their new environment, were momentarily thrown out of statistical equilibrium. Subsequent equilibration among the various species took place in a relaxation zone starting just behind the pulse or shock front.

A number of authors have studied this behavior in shock heated argon. Petschek and Byron[1] considered a flow where recombination of electrons and ions and radiation losses were neglected. Furthermore, they used a simplified energy balance relating changes of the free electron energy by elastic and inelastic encounters. Bond[2] included a simple model for both ionization and recombination, but neglected radiation losses in his total enthalpy balance. Harwell and Jahn[3] studied only the initial ionization rates, due to atom collisions, directly behind the shock front and concluded that ionization involved a two step procedure,

excitation prior to ionization. Wong[4] separated the relaxing flow into three regimes, the first located directly behind the shock front where collisions between atoms produce an initial supply of electrons, followed by the second where electron-atom collisions dominate the ionization processes, and finally the third beginning where recombination processes become appreciable. He noted that intense radiation became visible near the end of the relaxation zone and in the downstream quasi-equilibrium region, and that this radiation strongly affected the flow variables. His analysis, however, did not include such radiative effects and could not be applied to the strongly radiating quasi-equilibrium region.

The present study is designed 1. to gain a deeper understanding of the individual collisional and radiative processes within the flow and using this knowledge formulate a unified set of relations applicable not only to the relaxation zone but the downstream strongly radiating quasi-equilibrium region as well, and 2. extend this investigation into the shock layer preceding a cylinder-plate.

1.2 POSTULATED MODEL OF THE MICROSCOPIC FLOW PROCESSES

In order to understand the collisional and radiative phenomena within an argon plasma flow it is necessary to postulate a physical model of the microscopic processes occurring within the reacting gas. As the argon atoms pass through a strong shock front their thermal energy is greatly increased, within a few elastic collisions, to a value defined by the Rankine-Hugoniot relations. Subsequent inelastic collisions between these atoms result in their

electronic excitation and ionization and the production of an initial supply of free electrons at low thermal energies. Due to the large mass difference between the atoms, or ions, and the electrons, the latter must rely on inelastic collisions with excited atoms, i.e., superelastic collisions, as well as elastic encounters with atoms in order to gain substantial thermal energy. The resultant high energy free electrons may now interact inelastically with atoms, exciting or ionizing them, and thereby increasing the supply of free electrons in the gas. Once a substantial number of such electrons are available to give a degree of ionization of the order of 10^{-3}, the relatively large electron-atom inelastic cross-section as well as the high mobility of the electrons enable electron-atom inelastic encounters to serve as the dominant ionization process.

The argon atom in its ground energy state has its outermost subshell of electrons, the 3p subshell, completely filled. Upon excitation of the atom one of these electrons, denoted as the optical electron, transits into a higher energy orbit about the nucleus (see Fig. 1). Only one such optical electron is assumed to exist per atom. These higher energy levels are quickly populated within a region close to the shock front mainly by inelastic collisions between atoms. Some of the optical electrons acquire sufficient energy to enable them to leave the influence of the atomic nucleus, resulting in ionization of the atom. Quantitative analyses of the processes occurring in this region are difficult, and as yet insufficient information about them is available. However, as mentioned previously, once a significant number of free electrons are present their interactions with atoms

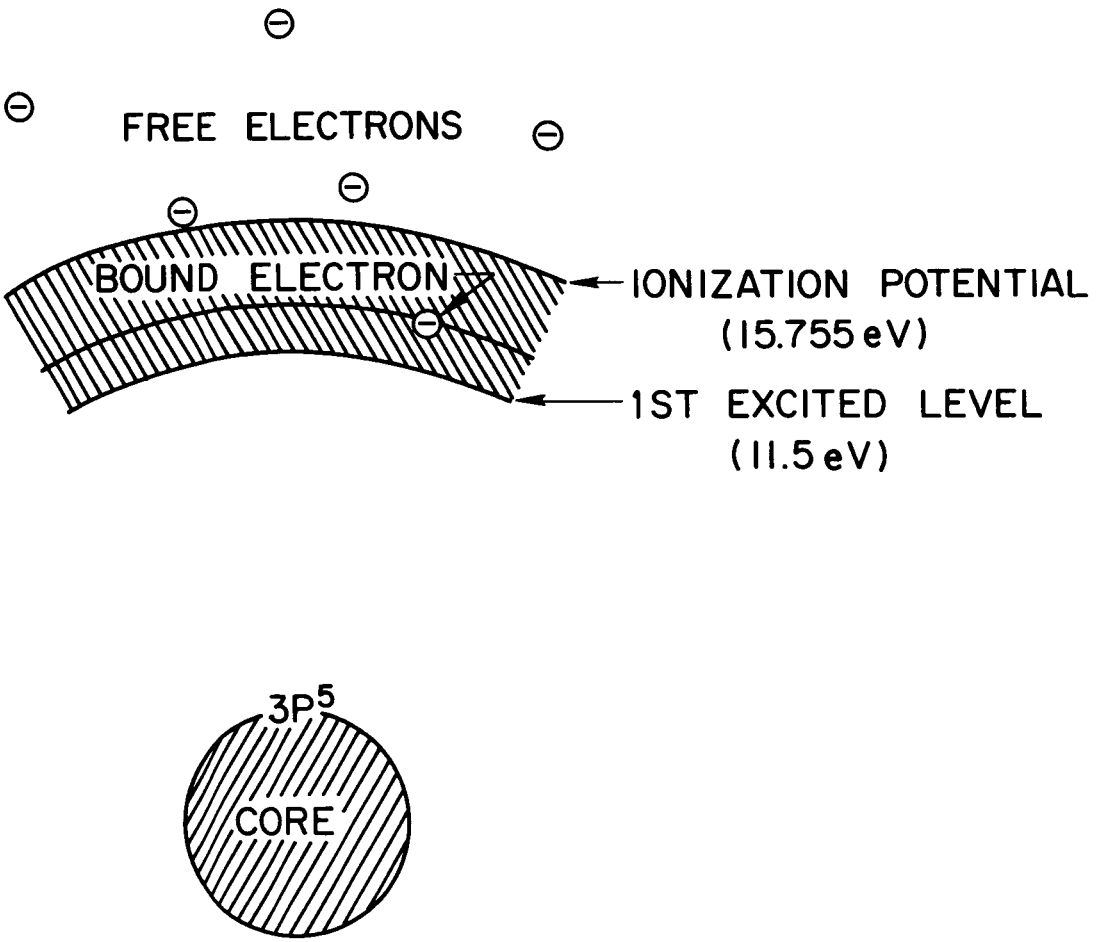

FIGURE 1. Excited Argon Atom

dominate the excitation and ionization processes. Under such conditions the heavy particles (atoms and ions) and the electrons separately suffer sufficiently numerous collisions to result in Maxwellian distributions of their thermal energies at, respectively, temperatures of T_A and T_e. Furthermore, since the first excitation level of argon exists at 11.5 ev above the ground state and the undisturbed ionization limit exists at 15.755 ev, adequate inelastic collisions are assumed to occur between the free electrons and the excited atoms to maintain the number densities of all excited levels of the atom in a Maxwellian distribution at the electron temperature.

1.3 AUTOIONIZATION, IONIZATION POTENTIAL LOWERING, SERIES TRUNCATION OF THE PARTITION FUNCTIONS, AND EFFECT OF IMPURITIES

To complete this description of the particle interactions some consideration must be given to 1) the phenomenon of autoionization, 2) the lowering of the ionization potential by electric microfields within the gas, 3) the number of atomic and ionic excitation levels to be considered, and 4) the effect of impurities on the rate of electron production.

Autoionization exists because there are two series limits for the ionization energy, corresponding to the two ground state configurations of the ion with total angular momentum quantum numbers $J_c = \frac{1}{2}, \frac{3}{2}$. Since these limits only differ by 0.178 ev autoionization has been assumed to have little influence on the rate of electron production and, therefore, is neglected in this study.

Lowering of the ionization limit, which affects the production rate of free electrons, is caused by the microfields within the plasma. A stationary electric field will split an atomic energy level into numerous discreet components (Stark effect). If such a field is caused by a number of perturbers in motion about the atom, the resultant microfield will change with time in both magnitude and direction. This causes the upper levels of the perturbed atom to be smeared out rather than be split into distinct components, thereby effectively broadening these levels. If such broadening is substantial enough to enable these levels to overlap into the continuum the ionization limit is lowered. Though numerous theories have been proposed to explain this phenomenon, there is a general lack of agreement between them, and it seems that only experimental evidence can resolve the confusion. In Section 5.2 there is some discussion on use of the shock tube as a possible tool for such experimental measurements. In the present study an Ecker-Weizel type of polarization relation is used, which is in close agreement with the concepts of many modern theorists. The result, as given by Pomerantz,[5] is

$$\Delta I = 0.38 \left[\frac{n_e}{T_e (10^{14})} \right]^{1/2}$$

where n_e is the number of electrons per cm^3 and ΔI is the lowering of the ionization limit in electron volts.

The number of electronic energy levels assumed for the atom and the ion affects the values of their partition functions, consequently influencing the population density of each of these levels.

In this study the ion is considered to exist only in its two ground levels so that its partition function, $Q_i(T_e)$, is given by,

$$Q_i(T_e) = 4 + 2 \exp\left(-\frac{2060}{T_e}\right)$$

For the atom the energies of the first few excited levels are known and higher levels are considered to obey a hydrogenic model. Since this would imply a diverging partition function, it is necessary to truncate the series, the "cutoff" occurring where the energy level of the last term of the series corresponds to the microfield lowered ionization limit. In the event that these microfields are too weak to provide sufficient lowering of the ionization limit, as occurs at the low electron densities directly behind an incident shock front, the maximum energy level is taken to correspond to a hydrogenic orbit whose radius is half the distance between adjacent atoms.

That impurities shorten the equilibration process is generally agreed, but the degree to which they affect the electron production rate is as yet unknown. Wong,[4] Harwell and Jahn,[3] and Petschek and Byron,[1] among others feel that the effect is appreciable in reducing the electronic relaxation time behind an incident shock. This subject is discussed in greater detail in Section 5.1.

1.4 FLOW PROBLEMS INVESTIGATED

With the foregoing description of the atom and its interactions, collisional as well as radiative effects can be calculated. The latter,

due to free-free (bremsstrahlung), free-bound and bound-bound electronic transitions are found to play a significant role in the quasi-equilibrium region downstream of the relaxation zone. Incorporation of these microscopic effects with the macroscopic conservation laws into a mathematical formulation enables definition of the flow of a nonequilibrium, radiating argon plasma behind a strong normal incident shock front.

Chapter 2 contains the theoretical description of the flow through a non-attenuating planar shock wave and constitutes the main analytical portion of this study. Chapter 3 considers the shock layer preceding a cylinder-plate, wherein the gas particles already heated and partially ionized by their passage through the incident shock, experience an additional change of conditions in traversing the shock layer preceding the cylinder.

1.5 EXPERIMENTAL MEASUREMENTS

The experimental results are obtained from both still and time resolved interferograms of the ionized argon flow. This technique has long been used in mapping gaseous densities, and is dependent upon the changes in the index of refraction of the working gas. Since this index is relatively insensitive to the impressed optical wavelength for the heavy particles while being highly dispersive for electrons, Alpher and White[6] were able to show in 1959 that dual wavelength optical interferometry could be used to measure independently the heavy particle and electron densities at any point within an ionized gas. These measurements are not dependent on the state of the gas

and therefore offer a technique of obtaining particle and electron densities irrespective of the degree of local thermal equilibrium. The experimental equipment and its operation are explained in Chapter 4, and the empirical results discussed and compared to the theoretical calculations in Chapter 5.

The present study is part of a long range investigation, being conducted at Stanford University, to gain a broader and deeper understanding of the dynamics of high temperature plasma flows, and the kinetics of their microscopic collisional and radiative processes.

CHAPTER 2

MATHEMATICAL RELATIONS GOVERNING THE FLOW BEHIND A STRONG NORMAL SHOCK FRONT

2.1 GENERAL AND TIME-INDEPENDENT, ONE-DIMENSIONAL FORMULATIONS

The following is a Lagrangian formulation of the equations governing a non-equilibrium, radiating argon plasma flow.

Conservation of Mass:
$$\rho \frac{D}{Dt}\left(\frac{1}{\rho}\right) = \frac{\partial u_j}{\partial x_j}$$

Conservation of Momentum:
$$\rho \frac{Du_j}{Dt} = -\frac{\partial p}{\partial x_j}$$

Conservation of Energy:
$$\frac{D}{Dt}\left(h_g + \frac{1}{2}u^2\right) = -\frac{q_R}{\rho} + \frac{1}{\rho}\frac{\partial p}{\partial t}$$

Thermal Equation of State:
$$p = n_e kT_e + (n_i + n_A)\, kT_A$$

Rate of Electron Production:
$$\frac{D}{Dt}\left(\frac{n_e}{\rho}\right) = Fn_A \text{ (collisional processes)}$$

Electron Thermal Energy Gain:
$$\frac{D}{Dt}\left(\frac{\frac{5}{2} n_e kT_e}{\rho}\right) = Fn_B$$

(collisional energy transfer between species)

where q_R, the rate of radiant energy loss per unit volume, and the

functions Fn_A and Fn_B are as yet undefined.

It must be noted that in this formulation volume forces, viscosity, and relative diffusion between species have been neglected.

In investigating the relaxation phenomenon behind a non-attenuating, strong normal shock front, and neglecting multi-ionization of atoms, the above formulation can be reduced to the following set of time-independent, one-dimensional relations with respect to a coordinate system travelling at the velocity of the shock front.

Conservation of Mass: $\rho u = \rho_r u_r$

Conservation of Momentum: $p + \rho u^2 = p_r + \rho_r u_r^2$

Conservation of Energy: $u \frac{d}{dx} \left(h_g + \frac{1}{2} u^2\right) = - \frac{q_R}{\rho}$

Thermal Equation of State: $p = \rho R(T_A + \alpha T_e)$

Rate of Electron Production: $u \frac{d}{dx} \left(\frac{ne}{\rho}\right) = Fn_A$ (collisional processes)

Electron Thermal Energy Gain: $u \frac{d}{dx} \left(\frac{\frac{5}{2} n_e k T_e}{\rho} \right) = Fn_B$

(collisional energy transfer between species)

where the subscript r refers to reference conditions.

The algebraic relations for conservation of mass and momentum are derivable from macroscopic considerations, where the momentum loss due to radiation has been neglected. The thermal equation of state

results from the kinetics of a two temperature partially ionized gas. The three remaining equations are seen to be differential and require for their full definition the investigation of the collisional and radiative processes within the gas. These will now be specifically formulated by using the atomic model described in Section 1.2 The resultant relations are applicable throughout the flow behind a normal shock front, except for the region close to the shock front dominated by atom-atom collisions where the excited levels of the atom have not yet attained a Boltzmann distribution at the temperature of the free electrons. However, application of these relations within this questionable region will probably produce insufficient deviations from the actual flow conditions to be observable experimentally.

2.2 CONSERVATION OF ENERGY

The enthalpy per unit mass of partially ionized argon gas is,

$$h_g = \frac{5}{2} R(T_A + \alpha T_e) + \frac{\alpha I}{m_A} + W$$

where the electronic energy of the excited states is denoted by W, and the radiation enthalpy of the gas has been neglected.

When the number densities of the excited levels of the atom are in thermal equilibrium at the temperature of the free electrons, W can be expressed as,

$$W = \frac{kh^3 \rho(\alpha T_e)^2}{2(2\pi m_e k T_e)^{3/2} m_A^2 Q_i(T_e)} \frac{dQ(T_e)}{dT_e} \exp\left(\frac{I}{kT_e}\right)$$

The rate of radiative energy loss, q_R, due to bremsstrahlung, free-bound, and bound-bound transitions requires a detailed knowledge of the internal structure of the argon atom, the oscillator strengths of the allowable electronic transitions, and the optical depth for each of these transitions. Such an investigation was conducted by Horn,[7] and his results were applied to the present non-equilibrium formulation.

The radiative loss due to bremsstrahlung and free-bound transitions collectively is given by Horn[7] as,

$$q_c = \frac{D(\alpha\rho)^2}{m_A^2 T_e^{1/2}} \left(\nu_c + \frac{kT_e}{h}\right) Z_{eff}^2$$

where,

$$D \triangleq \frac{64 e^6 \pi^{3/2}}{3\sqrt{6}\, m_e^{3/2} k^{1/2} c^3}$$

and the cutoff frequency, ν_c, was taken as 2.85 ev corresponding to transitions to the second excited, or 4p, level of the atom. Transitions to the first excited level are suggested by the results of Lagar'kov and Yakubov[8] to be quite small. The effective nuclear charge, Z_{eff}, was set at $\sqrt{1.5}$ in accordance with the theoretical work of Biberman and Norman[9] and the experimental work of Horn.[7]

The radiative loss due to bound-bound transitions is shown to be of the same order of magnitude as the loss due to transitions from the continuum, and is given by,

$$q_B = \frac{(\alpha\rho)^2 h^3 \exp(I/kT_e)}{2m_A^2(2\pi m_e kT_e)^{3/2} Q_i(T_e)} \sum_{q,p} M_{q,p} \exp\left(-\frac{E_{p,0}}{kT_e}\right)$$

where values for $M_{q,p}$ have been calculated by Horn.[7]

Summation of these two partial radiative losses results in an approximation for the total radiative emission and enables the differential relation for the conservation of energy to be expressed in terms of the flow variables.

2.3 RATE OF ELECTRON PRODUCTION

Initially electrons are produced by atom-atom inelastic encounters. When a substantial quantity of free electrons is available electron-atom inelastic encounters predominate. These will be treated in reverse order.

2.3.1 ELECTRON-ATOM INELASTIC ENCOUNTERS

2.3.1.1 GENERAL FORMULATION

The rate of electron production due to electron-atom encounters can be determined when sufficient free electrons are present so that the excited levels of the atom are thermally equilibrated at the electron temperature. The method used is based on that originally outlined by Bates, Kingston, and McWhirter.[10] Their theory, though developed for hydrogen atoms or hydrogenic ions was adapted to argon atoms having one optical electron.

Consider the following reactions in the gas,

Ionization and Three Body Recombination:

$$A(p) + e^- \underset{K(z,p)}{\overset{K(p,z)}{\rightleftharpoons}} A^+ + e^- + e^-$$

Collisional Excitation and De-excitation:

$$A(p) + e^- \underset{K(q,p)}{\overset{K(p,q)}{\rightleftharpoons}} A(q) + e^-$$

Photoionization and Radiative Recombination:

$$A(p) + h\nu \underset{\beta(z,p)}{\overset{\beta(p,z)}{\rightleftharpoons}} A^+ + e^-$$

Spontaneous Transitions:

$$A(p) \xrightarrow{\bar{A}(p,q)} A(q) + h\nu$$

Stimulated Emission and Absorption:

$$A(p) \underset{\bar{B}(q,p)}{\overset{\bar{B}(p,q)}{\rightleftharpoons}} A(q) + h\nu$$

where the rate coefficients for the forward and backward reaction processes are defined symbolically for transitions between two bound states, p and q, or one bound state and the continuum, p and z. $\bar{A}$ and $\bar{B}$ represent the Einstein coefficients for spontaneous and stimulated transitions.

These relations enable the rate of change in the number density of atoms having optical electrons in the p^{th} level to be expressed as

$$\frac{dn(p)}{dt} = -n(p)\{n_e[K(p,z) + \sum_{q\neq p} K(p,q)] + \sum_{q<p} \bar{A}(p,q) + \sum_{q\neq p} \rho_R(\nu_{p,q})\bar{B}(p,q)$$

$$+ \rho_R(\nu_{p,c})\ \beta(p,z)\} + n_e \sum_{q\neq p} n(q)\ K(q,p) + \sum_{q>p} n(q)\ \bar{A}(q,p)$$

$$+ \sum_{q\neq p} \rho_R(\nu_{q,p})\ n(q)\ \bar{B}(q,p) + n_e^3\ K(z,p) + n_e^2\ \beta(z,p)$$

If it is assumed that there are sufficient inelastic collisions to maintain the number densities of all the excited levels of the atom in thermal equilibrium with the free electrons, no additional optical electrons are able to transit into any excited orbits without upsetting the statistical balance of the gas. Therefore, for a given electron temperature, any jump of a ground state electron into an excited level must be accompanied by the transition of an excited electron into the continuum, and the mechanism for the recombination of a free electron must be analogous. However, since the electron temperature is not a static function, the number densities of the excited levels are not fixed quantities and subject to change, though the rate of such changes is small when compared to that of the ground level. This can be expressed mathematically as,

$$\sum_{p\neq 0} \frac{dn(p)}{dt} \ll \frac{dn(0)}{dt}$$

where $p = 0$ represents the ground level of the atom, and implies that,

$$\frac{dn(0)}{dt} \simeq - \frac{dn_e}{dt}$$

Furthermore, if the assumption is made that almost all of the ionization occurs from excited levels, and very little directly from the ground state, and that recombination follows a similar multi-step procedure, the rate coefficients $K(0,z)$, $\beta(0,z)$, $K(z,0)$ and $\beta(z,0)$, defining a one-step process between the ground state and the continuum, can be neglected.

In addition, the number density of an excited level, q, can be related to the electron density by a development similar to that employed in the derivation of the Saha equation. The resultant expression is,

$$n(q) = \frac{n_e^2 h^3}{2(2\pi m_e kT_e)^{3/2}} \frac{g(q)}{Q_i(T_e)} \exp\left(\frac{I - E_{q,0}}{kT_e}\right)$$

where $g(q)$ is the statistical weight of the q^{th} electronic energy level of the atom. This modified Saha relation was arrived at independent of whether the number densities of the ground state and the excited levels are in thermal equilibrium.

Summing the previous equation over all values of q, the total number density of atoms in all excited levels, becomes

$$\sum_{q>0} n(q) = \frac{n_e^2 h^3 \left[Q(T_e) - 1\right]}{2(2\pi m_e kT_e)^{3/2} Q_i(T_e)} \exp\left(\frac{I}{kT_e}\right)$$

and enables the number density of atoms in the ground state to be expressed as,

$$n(0) = \frac{\rho}{m_A} - n_e - \frac{n_e^2 h^3 [Q(T_e) - 1]}{2(2\pi m_e kT_e)^{3/2} Q_i(T_e)} \exp\left(\frac{I}{kT_e}\right)$$

These relations and the foregoing approximations transform the equation defining the rate of change of the number density of atoms in the ground state into the following form,

$$\frac{dn_e}{dt} \simeq n_e \left[\frac{\rho}{m_A} - n_e - \frac{n_e^2 h^3 [Q(T_e) - 1]}{2(2\pi m_e kT_e)^{3/2} Q_i(T_e)} \exp\left(\frac{I}{kT_e}\right)\right]$$

$$\times \sum_{q > 0} \left[K(0,q) + \frac{\rho_R(\nu_{0,q})}{n_e} B(0,q)\right]$$

$$- \frac{n_e^3 h^3 \exp(I/kT_e)}{2(2\pi m_e kT_e)^{3/2} Q_i(T_e)} \sum_{q > 0} g(q)\left[K(q,0) + \frac{1}{n_e} \bar{A}(q,0) + \frac{\rho_R(\nu_{q,0})}{n_e} \bar{B}(q,0)\right] \exp\left(-\frac{E_{q,0}}{kT_e}\right)$$

where the Einstein coefficients $\bar{A}(q,0)$, $\bar{B}(q,0)$, and $\bar{B}(0,q)$ and the excitation and de-excitation rate coefficients $K(0,q)$ and $K(q,0)$, as well as the radiation densities $\rho_R(\nu_{0,q})$ or their equivalent $\rho_R(\nu_{q,0})$, are as yet undetermined.

2.3.1.2 EVALUATION OF THE RADIATION DENSITIES AND THE EINSTEIN COEFFICIENTS

Consider first the terms containing the Einstein coefficients $\bar{B}(0,q)$ and $\bar{B}(q,0)$. Since these represent stimulated transitions

which are dependent on the radiation densities it is necessary to obtain an expression for these latter quantities. The following relation is derived in Appendix A for a body at temperature T in thermal equilibrium with its surroundings.

$$\rho_R(\nu) = \frac{4\pi}{c} B_\nu(T) \left[1 - \exp(-\tau_\nu)\right]$$

Using the Planckian distribution

$$B_\nu(T) = \frac{2\nu^3 h}{c^2} \left[\exp(\frac{h\nu}{kT}) - 1\right]^{-1}$$

the radiation density for a frequency ν is expressed as,

$$\rho_R(\nu) = \frac{8\pi\nu^3 h}{c^3} \frac{1 - \exp(-\tau_\nu)}{\exp(\frac{h\nu}{kT}) - 1}$$

where the optical depth $\tau_\nu = k_\nu x$ and x represents a characteristic length of the flow. It must be noted that only for black body radiation, where $\tau_\nu \to \infty$, is this condition of thermal equilibration exact and the above formula applies. For large τ_ν it is a good approximation.

The determination of the volume absorption coefficient, k_ν, requires an involved analysis, the details of which are shown in Appendix B for the singlet and triplet resonance transitions from the first excited, or 4s, level, at the resonance frequency, $\nu_{0,1}$. The results show that for a characteristic length, x = 5cm, corresponding to the width of the shock tube used in the experiments, the optical depths for the singlet and triplet transitions are respectively,

$$^{1}\tau_{\nu_{0,1}} = O[10^{5}] \quad \text{and} \quad ^{3}\tau_{\nu_{0,1}} = O[10^{4}]$$

Therefore, the gas can be considered optically thick for these resonance transitions enabling the radiation densities to be approximated by the Planckian form,

$$\rho_R(\nu_{0,1}) \simeq \frac{8\pi\nu_{0,1}^3 h}{c^3}\left[\exp\left(\frac{h\nu_{0,1}}{kT_e}\right) - 1\right]^{-1}$$

In addition to the radiation densities, the Einstein $\bar{A}$ and $\bar{B}$ coefficients must be determined. In Appendix C these latter quantities are related to another atomic constant, the oscillator strength, $f_{p,q}$, where p and q represent any two bound energy levels. The results are,

1) $$\bar{A}(p,q) = \frac{8\pi^2 e^2 \nu_{p,q}^2}{m_e c^3}\frac{g(q)}{g(p)} f_{q,p}$$

2) $$\bar{B}(q,p) = \frac{\pi e^2}{m_e h\nu_{q,p}} f_{q,p}$$

3) $$g(q)\,\bar{B}(q,p) = g(p)\,\bar{B}(p,q)$$

It is now possible to estimate values for the terms in the rate equation which include the Einstein coefficients. Consider first the summation,

$$\sum_{q>0} g(q)\,\bar{A}(q,0)\exp\left(-\frac{E_{q,0}}{kT_e}\right)$$

The first terms of this summation represent the singlet and triplet transitions from the $3p^5 4s$, or first excited level $(q = 1)$, to the ground state. Since the oscillator strengths for these transitions have been calculated by Knox[12] from the quantum mechanical Hartree-Fock relations, values of the Einstein $\bar{A}(1,0)$ coefficients can be calculated to be,

$$^1\bar{A}(1,0) = 4.0(10^{-8}) \text{ sec}^{-1} \qquad \text{and} \qquad ^3\bar{A}(1,0) = 0.98(10^{-8}) \text{ sec}^{-1}$$

In the second excited level $(q = 2)$, the optical electron travels in the $4p$ orbit and the atom can exist in ten j states. However, only four of these allow transitions to the ground level and, by the transition rules, they must have values of $j = 1$ with degeneracies of 3. Therefore, the function $g(q) \exp(-E_{q,0}/kT_e)$ decreases with increasing excited levels. Furthermore, Olsen[13] measured larger $\bar{A}$ values for neutral argon (argon I) transitions between the second and first excited levels than between the third and first excited levels. Logically this seems plausible, in that a one level quantum jump seems more probable than one spanning two levels. Assuming the validity of this hypothesis for resonance transitions, it follows that,

$$\bar{A}(q,0) < \bar{A}(1,0) \qquad \text{for} \quad q > 1$$

Therefore, due to the rapid decrease of the exponential function, resonance transitions, other than those from the first excited level, are neglected. This leads to the approximation,

$$\sum_{q>0} g(q)\,\bar{A}(q,0)\exp\left(-\frac{E_{q,0}}{kT_e}\right)$$

$$\simeq 3(10^{-8})\left[4.0\exp\left(-\frac{1.893(10^{-11})}{kT_e}\right)+0.98\exp\left(-\frac{1.859(10^{-11})}{kT_e}\right)\right]$$

Consider next the summations involving the Einstein $\bar{B}$ coefficients,

1) $$\sum_{q>0}\rho_R(\nu_{0,q})\,\bar{B}(0,q)$$

2) $$\sum_{q>0} g(q)\,\rho_R(\nu_{q,0})\,\bar{B}(q,0)\exp\left(-\frac{E_{q,0}}{kT_e}\right)$$

With the radiation density for each of these resonance transitions expressible in the Planckian form, it can be shown that for the conditions of this experimental investigation, where the maximum T_e is approximately 1 ev,

$$\frac{d[\rho_R(\nu)]}{d(\frac{h\nu}{kT_e})} < 0$$

so that,

$$\rho_R(\nu_{0,q}) < \rho_R(\nu_{0,1}) \qquad \text{for} \quad q > 1$$

Furthermore, since $\bar{A}(q,0) < \bar{A}(1,0)$, for $q > 1$, the Einstein relations show that,

1) $\bar{B}(q,0) < \bar{B}(1,0)$

2) $\bar{B}(0,q) < \bar{B}(0,1)$ for $q > 1$

where for allowable transitions the q levels must have degeneracies 3.

Consequently, by using an argument similar to that for obtaining an expression for the summation involving Einstein $\bar{A}$ coefficients, the terms involving the Einstein $\bar{B}$ coefficients can be approximated by the resonance transitions from the first excited level. Since the oscillator strengths for these transitions are known, the $\bar{B}$ coefficients are calculated to be,

$$^{1}\bar{B}(1,0) = 277 \text{ cm gm}^{-1} \qquad \text{and} \qquad ^{3}\bar{B}(1,0) = 71.35 \text{ cm gm}^{-1}$$

$$^{1}\bar{B}(0,1) = 831 \text{ cm gm}^{-1} \qquad \text{and} \qquad ^{3}\bar{B}(0,1) = 214.05 \text{ cm gm}^{-1}$$

and result in the approximations,

$$1) \quad \sum_{q>0} \rho_R(\nu_{0,q})\, \bar{B}(0,q) \simeq 831\, \rho_R[\nu = 2.86(10^{15}) \text{ sec}^{-1}] + 214.05\, \rho_R[\nu = 2.81(10^{15}) \text{ sec}^{-1}]$$

$$2) \quad \sum_{q>0} g(q)\, \rho_R(\nu_{q,0})\, \bar{B}(q,0) \exp\left(-\frac{E_{q,0}}{kT_e}\right)$$

$$\simeq 831\, \rho_R[\nu = 2.86(10^{15}) \text{ sec}^{-1}] \exp\left(-\frac{1.893(10^{-11})}{kT_e}\right) + 214.05\, \rho_R[\nu = 2.81(10^{15}) \text{ sec}^{-1}] \exp\left(-\frac{1.859(10^{-11})}{kT_e}\right)$$

2.3.1.3 THE EXCITATION AND DE-EXCITATION RATE COEFFICIENTS

Finally, suitable expressions for the summations of the excitation and de-excitation rate constants, $\sum_{q>0} K(0,q)$ and $\sum_{q>0} K(q,0)$ must be obtained.

Figure 2 is a plot of experimentally determined ionization cross-sections for electron-atom collisions obtained from Petschek and Byron[1] and based on the experimental data of Maier-Leibnitz. Since the ionization mechanism is considered to be a multi-step process whereby an electron is first raised to an excited level prior to being ionized, each of these measured ionization cross-sections in reality represents the summation of all the cross-sections for excitation from the ground level. A second degree polynomial weighted fit to the experimental results, adjusted to give the correct threshold, produces,

$$\sigma_{e\text{-}A}(\epsilon) = 8.183(10^{-19})\,\epsilon^2 - 1.536(10^{-17})\epsilon + 6.840(10^{-17})$$

where the inelastic cross-section, $\sigma_{e\text{-}A}(\epsilon)$, is in cm^2 and the energy, ϵ, of the colliding electron is in electron volts.

Since the thermal velocity of the electrons greatly exceeds that of the atoms in the region where electron-atom encounters dominate the collisional processes, the atoms are assumed to be stationary with respect to the colliding electrons. Consequently, the summation of the excitation rate coefficients can be represented by,

$$\sum_{q>0} K(0,q) = \frac{1}{m_e} \int_{\epsilon_i}^{\infty} f(\epsilon)\, \sigma_{e\text{-}A}(\epsilon)\, d\epsilon$$

where ϵ is the thermal energy of the electron and where the lower limit of integration begins at the energy, ϵ_i, corresponding to the first excited level of the atom.

For thermally equilibrated free electrons the distribution function, $f(\epsilon)$, has a Maxwellian form and the integration yields

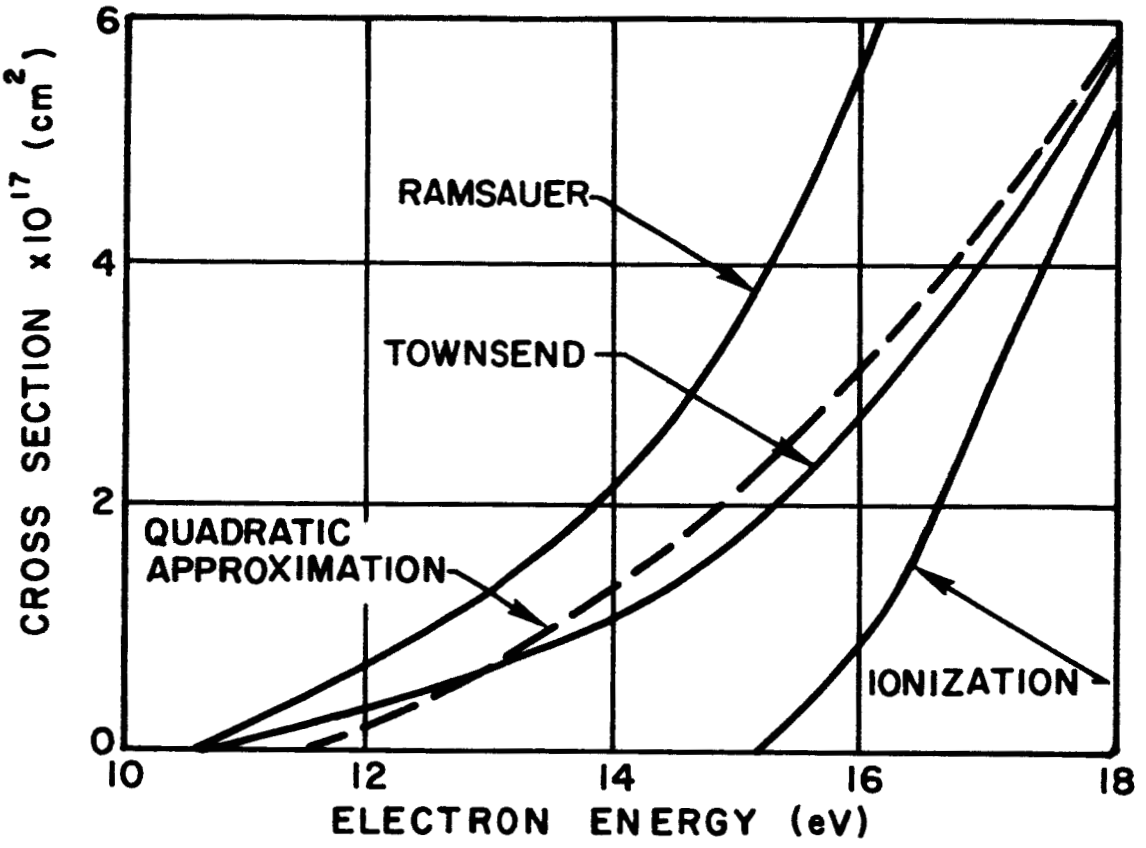

FIGURE 2. Electron-Atom Inelastic Cross-Section for Ground State Excitation

$$\sum_{q>0} K(0,q) = 4\left(\frac{2kT_e}{\pi m_e}\right)^{1/2}\left[-3.0(10^{-3})\left(\frac{m_e}{2kT_e}\right) + 2.07(10^{-17}) + 3.68(10^{-33})\left(\frac{2kT_e}{m_e}\right) + 1.985(10^{-49})\left(\frac{2kT_e}{m_e}\right)^2\right] \times \exp\left(-\frac{4.045(10^{16})m_e}{2kT_e}\right)$$

The de-excitation cross-section can be related to the excitation cross-section as shown by Seaton,[14] or by the method of detailed balancing outlined in Appendix D, and results in the following relation between the excitation and de-excitation rate coefficients,

$$\sum_{q>0} K(0,q) = \sum_{q>0} g(q)\, K(q,0) \exp\left(-\frac{E_{q,0}}{kT_e}\right)$$

The right hand side of this expression represents the de-excitation term required in the rate equation.

2.3.2 ATOM-ATOM INELASTIC ENCOUNTERS

Recognition must be given to the role of atom-atom inelastic encounters which produce the initial supply of free electrons behind the incident shock front. Theoretical and experimental information on the cross-sections for such encounters in argon are scarce. Sluyters et al.[15] conducted beam experiments in the high energy range of 5 to 24 kev, while Harwell and Jahn[3] attempted to measure such cross-sections for relatively low energies, approximating 1 ev, by microwave studies in shock tubes. Harwell and Jahn found that for shock

heated argon at an initial pressure of 5 mm Hg, the ionization mechanism proceeds in at least two steps, excitation followed subsequently by ionization. These results were based on a cross-section of the form,

$$\sigma_{A\text{-}A}(\epsilon) = c_1(\epsilon - \epsilon_i)$$

where c_1 is a constant, ϵ is the relative energy of a pair of colliding atoms relative to axes moving with their center of mass, and ϵ_i is the energy of the first excited level of the atom. Furthermore, at energies below 1 ev the electron production rate due to atom-atom encounters can be approximated by an Arrhenius dependence on the atom temperature and the energy of the first excitation level, which implies that electronic excitation to this level is the rate controlling reaction.

In the present study, where atom temperatures ranged up to 3 ev, such an Arrhenius dependence was included and a constant preceding the exponential was arbitrarily varied until the electronic relaxation length agreed with the experimental results. Such variations only changed the length of the relaxation zone and not the shape of its fringe profile. An example of this is shown in Fig. 12. Though, the number of experimental cases was limited, there was indication that the constant myltiplying the exponential would in reality have to be temperature dependent, thereby excluding a simple Arrhenius expression.

With this in mind the atom-atom collisional cross-section was investigated to determine what type of profile might be expected.

According to Massey and Burhop,[16] if the time during which an encounter takes place is much longer than the time required for an electron orbit, the electron can adjust to the perturbing conditions, thereby minimizing the probability of sufficient energy exchange for a quantum transition. Mathematically expressed, this "adiabatic" condition exists when,

$$\frac{r\Delta E}{hv} \gg 1$$

where r is the range of interaction between atoms, and v is their relative velocity.

For argon the first transition corresponds to a quantum energy jump, ΔE, of 11.5 ev. Therefore, with a lower limit on r of the order of 10^{-8} cm, a solution can be obtained for the relative velocity, v_0, and the corresponding energy, ϵ_0, at which the above relation is of the order of 1, i.e., when the probability of a transition to the first excited level becomes significant. This results in an ϵ_0 of the order of 1 kev so that the initial portion of the cross-section curve may be expected to resemble,

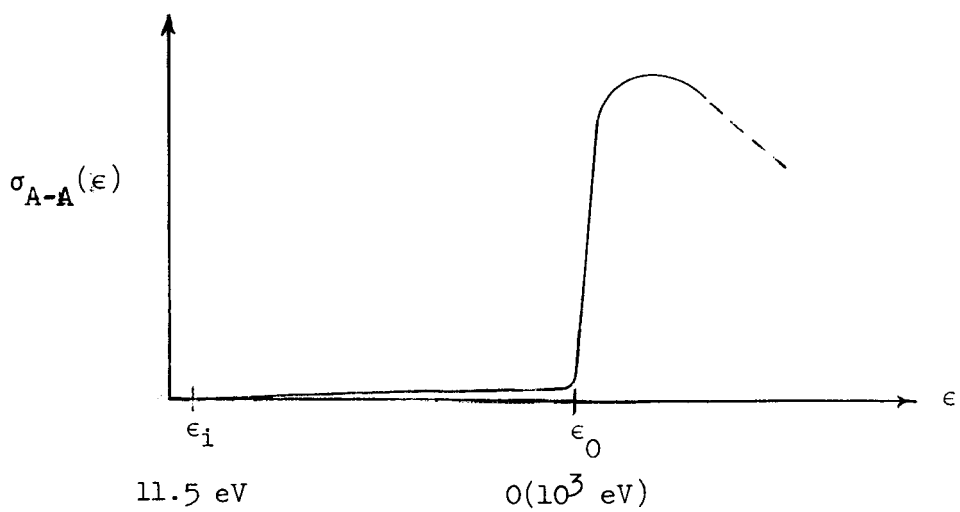

In a gas of atom temperatures below 3 ev, where there are extremely few atoms in the Maxwellian distribution with energies above 1 kev, most of the excitation and subsequent ionization must result from the high frequency of encounters by low energy atoms, even though the probability of a transition to the first excited level per such encounter is small. As most of the atoms are in an energy range near the ionization threshold, the initial portion of the cross-section curve, near the excitation energy, is of greatest interest.

Assume that the initial portion of the curve can be approximated by a polynomial of degree n,

$$\sigma_{A\text{-}A}(\epsilon) = \sum_{m=1}^{n} c_m(\epsilon - \epsilon_i)^m$$

where the excitation energy $\epsilon_i = \frac{1}{4} m_A v_i^2$, and the c_m's are constants. Using the relation given by Chapmann and Cowling[17] for the collision frequency together with the above expression for the inelastic cross-section, the following representation for the electron production rate due to atom-atom inelastic encounters is developed in Appendix E,

$$\frac{D}{Dt}\left(\frac{n_e}{\rho}\right)_{A\text{-}A} = \frac{2\rho(kT_A)^{1/2}}{(m_A)^{5/2}\,\pi^{1/2}}\left[\sum_{m=1}^{n} c_m(m+1)!\,(kT_A)^m\left(\frac{\epsilon_i}{(m+1)kT_A}+1\right)\right]\exp\left(-\frac{\epsilon_i}{kT_A}\right)$$

The constants c_m, and the number of terms, n, required must be determined by equating these theoretical production rates to those experimentally derived, by mating relaxation lengths, as described previously. Unfortunately, the limited number of experimental results

in this study did not enable accurate evaluation of the cross-section. A two term solution was attempted for four test cases. The values of c_1 and c_2 were of the order of 10^{-8} and 10^{3} respectively. A more precise quantitative analysis involving more terms is left for future investigation.

With an arbitrarily chosen value for the electron production rate due to atom-atom inelastic encounters and the relations derived in section 2.3.1 the function Fn_A is defined and results in a ordinary, non-linear differential equation for the total rate of electron production.

2.4 RATE OF THERMAL ENERGY GAIN BY THE FREE ELECTRONS

The rate of thermal energy gain by the electron sub-flow constitutes a sixth independent relation defining the flow processes. It is obtained by considering the free electrons as being subjected to randomly directed elastic and inelastic encounters with the atoms and ions. Since diffusion of the various species has been neglected, such encounters only change the enthalpy of the electron sub-flow. If this enthalpy is expressed as,

$$h_e = e_e + \frac{p_e}{\rho} = \frac{\frac{5}{2} n_e kT_e}{\rho}$$

the resultant rate of energy transfer to the free electrons becomes,

$$\frac{D}{Dt}\left(\frac{n_e T_e}{\rho}\right) = \frac{2}{5k}\left(\frac{\Phi}{\rho}\right)$$

where φ defines the rate of increase, per unit volume, of the electron thermal energy due to elastic and inelastic encounters with heavy particles. Comparison of this relation with the original Lagrangian formulation in Section 2.1 reveals that $\varphi \equiv (\rho)(Fn_B)$.

Neglecting multi-ionization of atoms and considering only the time-independent, one-dimensional case, the above relation is expressed as,

$$\frac{d}{dx}(\alpha T_e) = \frac{2m_A}{5k}\left(\frac{\varphi}{\rho_r u_r}\right)$$

where conservation of mass allows replacement of ρu by $\rho_r u_r$.

2.4.1 DETERMINATION OF THE RATE OF ENERGY GAIN, φ

The rate of thermal energy gain, φ, by the electron sub-flow is dependent on the following processes each of which is examined in detail.

2.4.1.1 ELASTIC ENERGY TRANSFER BY ELECTRON-ION ENCOUNTERS

Landau[18] investigated the elastic energy transfer between an electron and an ion during an encounter by considering only small deflections of the trajectory of the electron, with a resultant significant momentum change only in the direction perpendicular to the initial trajectory. By working in momentum space he obtained an expression for the rate of energy increase of a Maxwellian distribution of electrons, due to their encounters with ions, also in a Maxwellian distribution. His resultant relation involves the Debye length which,

for the conditions of this experiment, defines a Debye sphere containing approximately 4 electrons, and consequently too few to provide adequate shielding.[19] However, considering a sphere with radius twice the Debye length resolves this problem and the resultant expression becomes,

$$\varphi_1 = \frac{2n_e^2 e^4}{m_A} \left(\frac{8\pi m_e}{kT_e}\right)^{1/2} \left(\frac{T_A}{T_e} - 1\right) \ln\left(\frac{2d_D}{b_0}\right)$$

where the Debye length, d_D, is defined in line with most published works, as

$$d_D = \left(\frac{kT_e}{4\pi e^2 n_e}\right)^{1/2}$$

It must be noted that Cambel,[20] using the Debye-Hückel theory, wherein he includes the ion distribution, derives a Debye length for a singly ionized gas which is smaller by a factor of $\sqrt{2}$ than the above result. However, the higher mobility of the electrons enables them to dominate the shielding, thereby suggesting use of the standard definition in this study.

The closest approach, for elastic impact, between an electron and an ion is b_0 and can be obtained by equating the Coulombic and centrifugal forces between an electron-ion pair. This results in the following relation for a pair of colliding particles with average kinetic energy,

$$b_0 = \frac{e^2}{4kT_e}$$

and transforms the preceding modified Landau expression into,

$$\varphi_1 = \frac{(\alpha\rho)^2 e^4}{m_A^3} \left(\frac{8\pi m_e}{kT_e}\right)^{1/2} \left(\frac{T_A}{T_e} - 1\right) \ln\left[\frac{16(kT_e)^3 m_A}{\pi e^6 \alpha\rho}\right]$$

2.4.1.2 ELASTIC ENERGY TRANSFER BY ELECTRON-ATOM ENCOUNTERS

The rate of energy transferred to the electrons by the atoms during elastic encounters is given by de Voto[21] as,

$$\varphi_2 = 4kn_e(T_A - T_e)\left(\frac{8kT_e}{\pi m_e}\right)^{1/2} n_A \frac{m_e}{m_A} \sigma'_{e-A}(T_e)$$

A quadratic polynomial was fit to his plot of the average cross-section, $\sigma'_{e-A}(T_e)$, for such elastic encounters and resulted in transforming the above expression into,

$$\varphi_2 = \frac{4(10^{-16})(\alpha\rho)^2}{m_A^3}\left(\frac{T_A}{T_e} - 1\right)(kT_e)^{3/2}\left(\frac{8m_e}{\pi}\right)^{1/2}\left(\frac{1-\alpha}{\alpha}\right)$$

$$\times [-5.88(10^{-9})\ T_e^2 + 4.64(10^{-4})\ T_e - 0.337]$$

2.4.1.3 ENERGY LOSS DUE TO BREMSSTRAHLUNG

During their encounters with ions and atoms the acceleration of the electrons causes them to radiate energy (bremsstrahlung). Only such radiation due to electron-ion encounters has been considered, and the resultant rate of energy loss is given by Rose and Clark,[22] as,

$$\varphi_3 = \frac{8\pi}{\sqrt{6}} \frac{(\alpha\rho)^2 e^6\ kT_e}{m_e^2 m_A^2 c^3 h}\left(\frac{8\pi m_e}{kT_e}\right)^{1/2}$$

2.4.1.4 INELASTIC ENERGY TRANSFER BY ELECTRON-ATOM ENCOUNTERS

Thermal energy may be transferred to the free electrons by a variety of inelastic encounters with atoms. The following reactions are considered.

2.4.1.4.1 MULTI-STEP IONIZATION OF THE ATOM FROM ITS GROUND STATE

In this process the atom is first raised to an excited level due to either collisions with electrons or absorption of radiant energy, and then assumed to ionize through subsequent collisions with electrons. For such interactions, the following approximation for the resultant rate of energy loss from the electron sub-flow can be obtained,

$$\varphi_4 = \left[\frac{\rho}{m_A}(1-\alpha) - [Q(T_e)-1]\frac{n_e^2 h^3 \exp(I/kT_e)}{2(2\pi m_e kT_e)^{3/2} Q_i(T_e)}\right]$$

$$\times\left[\frac{\alpha\rho I}{m_A}\sum_{q>0} K(0,q) + 831\rho_R[\nu = 2.86(10^{15})\ \text{sec}^{-1}]\ E_{I,1}\right.$$

$$\left. + 214.05\rho_R[\nu = 2.81(10^{15})\ \text{sec}^{-1}]\ E_{I,1}\right]$$

where $E_{I,1}$ is the energy difference between the ionization potential and the first excited level of the atom.

2.4.1.4.2 TWO-BODY RADIATIVE RECOMBINATION

If an electron and an ion are to recombine without the presence of a third body, the electron must be within the minimum elastic impact distance, b_0, of the ion. Since $b_0 \propto 1/T_e$ and the

electron temperature in this study is at maximum slightly above 1 electron volt, the average spacing between electrons and ions is of the order of $100b_0$. Therefore, only those electrons in the Maxwellian distribution with energies of the order of 0.01 ev or below can experience two-body recombination. The expression for the fraction of electrons in a Maxwellian distribution with energies below a given value, E_R, can easily be derived and yields,

$$\frac{\Delta n_e}{n_e} = \text{erf}\,\Lambda - \frac{2}{\sqrt{\pi}}\,\Lambda \exp(-\Lambda^2)$$

where $\Lambda \triangleq (E_R/kT_e)^{1/2}$.

For $E_R = 0.01$ ev,

$$\frac{\Delta n_e}{n_e} \simeq 0.04\%$$

Since this percentage is small the thermal energy loss due to radiative recombination was neglected.

2.4.1.4.3 THREE-BODY COLLISIONAL RECOMBINATION

The assumption is made that in almost all collisions between two free electrons and an ion the recombining electron is bounded into one of the numerous energy levels near the ionization limit of the atom and the thermal energy it loses is gained by the other electron involved in the collision. Consequently, for this type of interaction there is essentially no change in the total thermal energy of the electron sub-flow.

2.4.1.4.4 COLLISIONAL DE-EXCITATION

In collisional de-excitation the electronic energy lost by an atom during its transition from an upper energy level, q, to a lower level, p, is gained by the colliding free electron. Since the number densities of the excited levels are assumed to be in thermal equilibrium, only transitions to the ground level, designated by $p = 0$, need be considered. This enables the rate of energy gain by the electron sub-flow for collisional de-excitation to be expressed as,

$$\varphi_5 = \frac{n_e^3 h^3 \exp(I/kT_e)}{2(2\pi m_e kT_e)^{3/2} Q_i(T_e)} \sum_{q>0} g(q)\, K(q,0)\, E_{q,0} \exp\left(-\frac{E_{q,0}}{kT_e}\right)$$

From the results of Appendix D,

$$\sum_{q>0} g(q)\, K(q,0)\, E_{q,0} \exp\left(-\frac{E_{q,0}}{kT_e}\right) = \sum_{q>0} E_{q,0}\, K(0,q) \equiv \bar{E}_{q,0} \sum_{q>0} K(0,q)$$

where the final equality can be introduced if $\bar{E}_{q,0}$ is defined as a weighted average energy. Assuming that $K(0,1) \gg K(0,2) \gg \cdots \gg K(0,m)$, $\bar{E}_{q,0}$ can be approximated by $E_{1,0}$, the energy of the first excited level. This enables the rate of energy gain of the electron gas by this process to be approximated by,

$$\varphi_5 \simeq \frac{n_e^3 h^3 \exp(I/kT_e)\, E_{1,0}}{2(2\pi m_e kT_e)^{3/2} Q_i(T_e)} \sum_{q>0} K(0,q)$$

2.4.1.5 INELASTIC ENERGY TRANSFER BY ATOM-ATOM ENCOUNTERS

The production of the initial free electrons behind the

incident shock front results from inelastic encounters between atoms. Empirical information on the thermal energy gained by these ionized electrons in such collisions seems practically non-existent, though it would seem probable that most of the collisional energy exchange is used for ionization and the resultant free electrons are relatively cold. However, a few experiments conducted at the University of Colorado[23] indicate that for strong cylindrical shock waves the initial electron thermal energy may be approximately equal to its equilibrium value at the end of the relaxation zone.

In the present theoretical formulation it was found that arbitrarily varying this initial value of the electron thermal energy did not affect the measurable quantities sufficiently to enable such deviations to be observed experimentally. Consequently, an expression was postulated whereby the electron production rate due to inelastic encounters between atoms was multiplied by a constant value, E_A, representing an assigned mean energy to these free electrons. This enabled the rate of energy gain by the free electrons due to such encounters to be expressed symbolically as,

$$\varphi_6 = E_A \left(\frac{dn_e}{dt} \right)_{\text{atom-atom collisions}}$$

The actual value of E_A was taken as somewhere between one-third and two-thirds of its value at the end of the relaxation zone.

Algebraic summation of these six component relations representing thermal energy gain by the free electrons due to their various

interactions results in the total thermal energy transfer, φ, and enables formulation of the final equation necessary to define the non-equilibrium flow. This resultant ordinary, non-linear differential equation, together with the other five relations and the Rankine-Hugoniot relations for the jump conditions across the shock front provide the complete set of expressions required for the definition of the relaxation and quasi-equilibrium regions behind a strong normal shock front propagating through argon gas.

CHAPTER 3

ANALYSIS OF THE SHOCK LAYER PRECEDING A CYLINDRICALLY BLUNT NOSED BODY

3.1 INTRODUCTION

A qualitative, predominantly experimental, investigation was conducted of the shock layer preceding a cylinder-plate. The discontinuity in conditions across the bow wave is analogous to the jump in conditions across an incident shock front and the Lagrangian formulation presented in Section 2.1 is equally applicable to the shock layer flow. Here, however, the coordinate system is attached to the model, so that the flow becomes time-dependent and two-dimensional. Consequently, the Lagrangian expressions reduce to a set of partial differential equations which cannot be handled as readily as were the time-independent, one-dimensional relations of Chapter 2.

The bow wave and shock layer were formed by passage over the model of the supersonic flow behind an incident shock front. Figures 29 through 34 show these shock layers for various incident shock strengths and distances behind the incident shock front. In most of these photographs there is definite evidence of an electronic relaxation zone behind the bow wave, followed by a region of intense radiation. The experimental results will be discussed more fully in Chapter 5, and the rest of this chapter will be devoted to a theoretical investigation of conditions along the stagnation streamline of the model.

3.2 INITIAL CONDITIONS

Calculation of the jump conditions across the bow wave requires quantitative knowledge of the upstream flow variables ahead of the wave. If this flow is in local equilibrium, then Glass and Kawada[24] show that the speed of sound, a_e, is

$$a_e^2 = \gamma_e \frac{p}{\rho} = \gamma_e(1 + \alpha)\, RT$$

where the equilibrium specific heat ratio, γ_e, can be expressed, from thermodynamic considerations, as,

$$\gamma_e = \frac{2}{(1+\alpha)(2-\alpha)} \; \frac{5(1+\alpha) + \alpha(1-\alpha^2)\left(\frac{5}{2} + \frac{I}{kT}\right)^2 + \frac{2}{R}\left(\frac{\partial W}{\partial T}\right)_p}{3(1+\alpha) + \frac{2\alpha(1-\alpha)}{2-\alpha}\left(\frac{3}{2} + \frac{I}{kT}\right)^2 + \frac{2}{R}\left(\frac{\partial W}{\partial T}\right)_V}$$

For the conditions of this experimental study the terms containing the partial derivatives of the electronic energy, W, can be neglected.

If the flow entering the bow wave emanates from the region downstream of the electronic relaxation zone behind the incident shock front, it will be in quasi-equilibrium so that $T_A = T_e \equiv T$. In such cases the preceding equilibrium speed of sound and specific heat ratio can be used. When, however, the bow wave is within the non-equilibrium relaxation zone behind the incident shock front, then the degree of ionization of the flow entering the bow wave can well be smaller than 10^{-3} and the electron temperature will be less than the heavy particle temperature. Under these conditions the assumption is made that the speed of sound and the specific heat ratio will depend primarily on the

properties of the heavy particles. Consequently, the following approximations can be made for the speed of sound and specific heat ratio in the flow behind the incident shock front, regardless of the degree of thermal equilibrium

$$a^2 \simeq \gamma(1 + \alpha)\, RT_A$$

where

$$\gamma \simeq \frac{2}{(1+\alpha)(2-\alpha)} \; \frac{5(1+\alpha) + \alpha(1-\alpha^2)\left(\frac{5}{2} + \frac{I}{kT_A}\right)^2}{3(1+\alpha) + \frac{2\alpha(1-\alpha)}{2-\alpha}\left(\frac{3}{2} + \frac{I}{kT_A}\right)^2}$$

and it is therefore possible to calculate a flow Mach number, $M = u/a$, within this region.

In passing through the bow shock front the following assumptions are made:

a) No inelastic energy is transferred between particles, so that the degree of ionization remains constant.

b) Virtually no elastic energy is transferred between the electrons and heavy particles, so that the electron temperature remains constant.

c) Charge neutrality is preserved, so that there is no diffusion of electrons upstream of the shock front.

d) The density jump through the shock front is determined by the properties of the heavy particles.

For a perfect gas the density jump across a normal shock front is given by the Rankine-Hugoniot relations as shown in Liepmann and Roshko,[25]

$$\frac{\rho_b}{\rho_a} = \frac{(\gamma+1)\, M_a^2}{(\gamma-1)\, M_a^2 + 2}$$

where a and b refer to upstream and downstream conditions respectively. By assumption d) this equation is considered to apply to an ionized gas when the previously derived relations for Mach number and specific heat ratio are used.

With α, ρ, and T_e known downstream of the bow shock front the other variables u, p and T_A can be calculated from the laws of conservation of mass and momentum, and the thermal equation of state.

3.3 TIME-INDEPENDENT, ONE-DIMENSIONAL FORMULATION

If the stream tube surrounding the stagnation streamline retains approximately constant area while traversing most of the shock layer, then the time-independent, one-dimensional equations derived in Section 2.1 can be applied in order to estimate the stagnation streamline flow within the shock layer. However, when such theoretical results for an incident Mach number of 11.32 are compared to the interferogram shown in Fig. 32 the theoretical electronic relaxation length within this layer is found to be much longer than experimentally observed. Consequently, such a constant area stream tube analysis in incorrect.

3.4 CONSTANT DENSITY FORMULATION

In order to retain ordinary differential equations a Lagragian formulation of the flow relations was attempted. By use of the conservation of mass and momentum relations the energy equation can be

converted into,

$$\frac{De_g}{Dt} + p \frac{D}{Dt}\left(\frac{1}{\rho}\right) = -\frac{q_R}{\rho}$$

where e_g represents the internal energy of the gas. This expression together with the Lagrangian relations derived in Chapter 2 for the rate of electron production, the rate of energy transfer between species, and the thermal equation of state, as well as the integrated form of Euler's equation for constant density,

$$p + \frac{1}{2}\rho u^2 = \text{constant}$$

constitute a determinate set of relations for calculating the conditions of the flow along streamlines. Measurements of mass density for an incident shock Mach number of 11.32 did indicate, as shown in Fig. 36, that in fact such density variations were small at the stagnation streamline. However, the theoretical solution showed that a gas particle would have to increase its velocity as it approached the surface of the model, an obviously invalid result. Consequently, the density along the stagnation streamline cannot be constant, suggesting possible errors in trying to evaluate this quantity from the polaroid interferograms.

No theoretical solutions involving one independent variable were obtained that agreed with the experimentally observed conditions along the stagnation streamline. In all probability a more extensive investigation is required involving two spatial variables, as discussed in Section 5.3.

CHAPTER 4

EXPERIMENTAL EQUIPMENT AND TECHNIQUE

4.1 INTERFEROMETRIC RELATIONS APPLICABLE TO IONIZED FLOWS

Consider a flow of particles comprising a polarizable species i. The complex refractive index of this flow is $(N_c)_i = N_i - i\bar{K}_i$, where N_i is the refractive index and $\bar{K}_i$ is the absorptivity of species i. The complex dielectric constant is $(\epsilon_c)_i = 1 + 4\pi n_i (\Psi_c)_i$ where n_i is the number density of species i and $(\Psi_c)_i$ is its complex polarizability with real and imaginary parts Ψ_i and $i\Psi_i'$. At the optical frequencies $(\epsilon_c)_i = (N_c)_i^2$, so that,

$$(N_c)_i - 1 \simeq 2\pi n_i (\Psi_c)_i$$

where only the first term of the binomial expansion is included. Equating the real parts of this relation,

$$N_i - 1 \simeq 2\pi n_i \Psi_i$$

The free electrons also contribute to the refractive index, and with the aid of Maxwell's equations and the equation of motion of a free electron this contribution in a tenuous plasma becomes,

$$N_{el} - 1 \simeq -\frac{1}{2}\left(\frac{\omega_p}{\omega}\right)^2$$

where the plasma frequency, ω_p, is given by, $\omega_p^2 = (4\pi n_e e^2)/m_e$ and the impressed optical frequency, $\omega \equiv 2\pi\nu$.

If the changes in refractivity due to the various particles are independent of one another, the total effect is the summation of the separate components,

$$\Delta(N - 1) = \sum_i \Delta(N_i - 1) + \Delta(N_{el} - 1)$$

Neglecting the contribution of excited levels the species i are composed of ground state atoms and ions, and electrons,

$$\Delta(N - 1) = \Delta(N_A - 1) + \Delta(N_{A^+} - 1) + \Delta(N_{el} - 1)$$

and the total fringe shift between any two regions 1 and 2 for an impressed wavelength, λ, and optical path length, L, is,

$$S_{1,2} = \frac{L}{\lambda} \Delta_{1,2}(N - 1) \simeq \frac{L}{\lambda} \Delta_{1,2} \left[2\pi n_A \psi_A + 2\pi n_{A^+} \psi_{A^+} - \frac{1}{2} \left(\frac{\omega_p}{\omega}\right)^2 \right]$$

$$S_{1,2} = \frac{L}{\lambda} (N_A - 1)_0 \frac{\rho_1}{\rho_0} \left\{ \left(\frac{\rho_2}{\rho_1} - 1 \right) + \left(\alpha_2 \frac{\rho_2}{\rho_1} - \alpha_1 \right) \left[\frac{\psi_{A^+}}{\psi_A} - 1 - \frac{1}{\psi_A m_e} \left(\frac{e\lambda}{2\pi c}\right)^2 \right] \right\}$$

where the subscript 0 refers to conditions at standard temperature and pressure. A curve of $(N_A - 1)_0$ versus wave length is shown in Fig. 3. The ratio of polarizabilities of the argon ion to the atom can be taken to be 0.67, as mentioned by Alpher and White.[6]

The Mach-Zehnder optical interferometer was used to measure the fringe shifts behind 1) the incident shock front, and 2) the bow wave preceding the cylinder-plate model. In the former case region 1 was denoted by conditions upstream of the incident shock front, and in

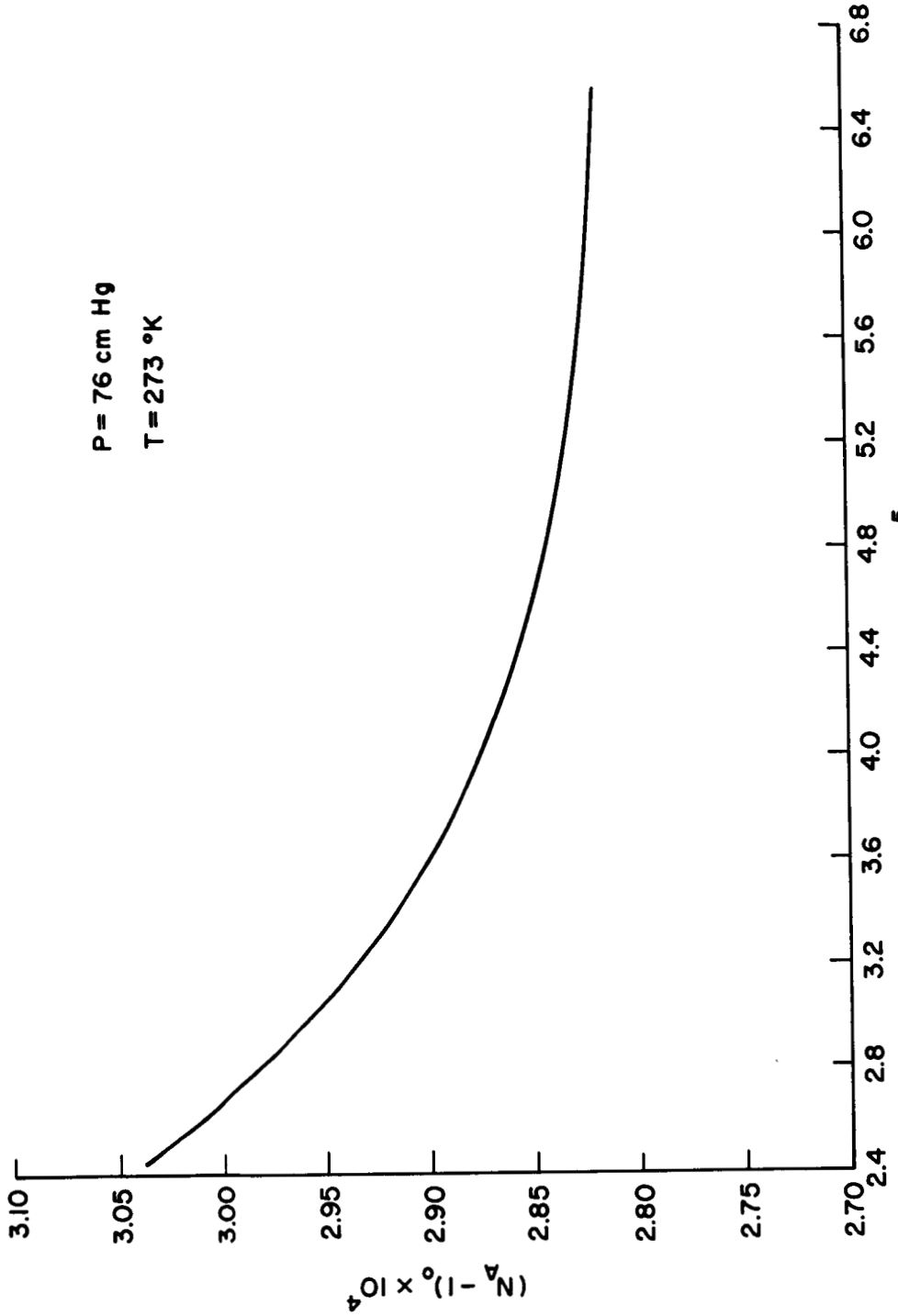

FIGURE 3. Refractivity of Atomic Argon

the latter case by conditions upstream of the bow wave. With the ground state polarizability of the atom given by

$$\Psi_A = \frac{(N_A - 1)_0 \, m_A}{2\pi\rho_0}$$

and conditions in region 1 known, measurements, at two optical wavelengths, of the fringe shifts at a point in region 2, behind the incident shock or the bow wave, enabled the density and degree of ionization to be calculated. The wavelengths chosen in this study, 4500 Å and 5890 Å, were sufficiently spread to enable good experimental accuracy to be obtained at an optical path length of 5 cm, the width of the shock tube.

4.2 THE SHOCK TUBE

The Stanford Aerophysics Laboratory shock tube, shown in Fig. 4, is of extruded aluminum, 25 feet in length with an interior cross-section two inches square and walls 0.75 inches thick. Figure 5 is a schematic representation of the shock tube and the adjoining instrumentation. Pumping stations located at each end of the tube evacuated the driven section to a pressure of the order of 10^{-5} mm Hg prior to filling it with argon. A stoichiometric mixture of hydrogen and oxygen, diluted with helium, was used as the driver gas and ignited by a series of spark plugs. The heated gas ruptured a prescribed aluminum diaphragm and sent the incident shock front down the driven section into the argon working gas. The test section and model, shown in Fig. 6, were located 20 feet downstream of the diaphragm. A pair of borosilicate crown glass optical windows, 2.75 inches in diameter, 0.75 inches thick, flat

to 0.25 wavelengths, and parallel to 0.0005 inches was used to view the flow, records of which were kept by a rotating mirror camera, shown in Fig. 7, or on polariod snapshots. Three barium titanate pressure transducers mounted flush with the shock tube walls and located upstream of the windows measured the incident shock velocity (see Fig. 8). A dump chamber at the end of the driven section and separated from it by a thin aluminum diaphragm which ruptured on contact with the shock, prevented wave reflection.

4.3 ADDITIONAL EQUIPMENT AND INSTRUMENTATION

The Mach-Zehnder interferometer, on loan through the courtesy of the Lockheed Missiles and Space Company Research Laboratories, is pictured in Fig. 9, and a schematic of the interferometric system is shown in Fig. 10.

The relaxation phenomenon behind the incident shock front was observed by use of the rotating mirror camera which recorded time resolved interferograms of the flow. An exploding 1 mil tungsten wire powered by a 7.5 $\mu\mu$fd Sangamo condenser charged to 20 kv provided a strong light source of over 100 μsec duration. The camera contained a stainless steel hexagonal mirror with faces ground flat to 0.5 wavelengths, and was spun by a gas powered turbine motor capable of reaching 80,000 r.p.m. A 3 inch, f-2.5 lens focused the light on the mirror, thereby sweeping the image of a slit portion of the flow, 1.5 inches high and 0.002 inches wide, over a strip of Royal X-pan film at sufficient speed to obtain time resolutions of 0.15 μsec.

A number of tests were conducted to investigate the shock layer preceding the 1/2 inch diameter cylinder-plate model. Still photographs of this layer were taken with Polaroid 3000 speed film while a Kerr cell with an electronic "shutter" speed of 5 μsec, manufactured by the Kappa Scientific Corporation, was used in place of the radiation stop in Fig. 10 to reduce overexposure from gaseous radiation.

In both the time resolved and most of the Polaroid photographs the images were split by two interference filters situated at the image plane of the test section. These filters, 4500 Å and 5890 Å, had band widths of 90 Å.

Two dual beam Tektronix oscilloscopes with Polaroid attachments were used to record both the incident shock speed and the time at which the Kerr cell opened.

4.4 EXPERIMENTAL TECHNIQUE

The shock tube and dump tank were pumped down for a minimum of two hours prior to the start of an experimental run. At the end of this period the pressure in the driven section was measured by an ionization gauge to be of the order of 10^{-5} mm Hg. This section was then filled with argon to a pressure between 3 and 5 mm Hg, depending on the run, after which a stoichiometric mixture of combustion gases was pumped into the driven section. The amounts of the component gases in this mixture depended on the desired shock velocity. Upon completion of the filling procedure the temperature of the driven section was

measured and the light source condenser charged. Then the angular velocity of the rotating mirror was stabilized at approximately 600 r.p.s. and the spark plugs discharged to ignite the combustion gases. The heated flow ruptured the main diaphragm sending an incident shock front through the driven gas. As the shock passed the barium titanate crystal gauges signals were sent to the oscilloscopes which recorded the shock velocity and triggered the light source condenser. When required, a magnetic field, produced by the discharging condenser, opened the Kerr cell.

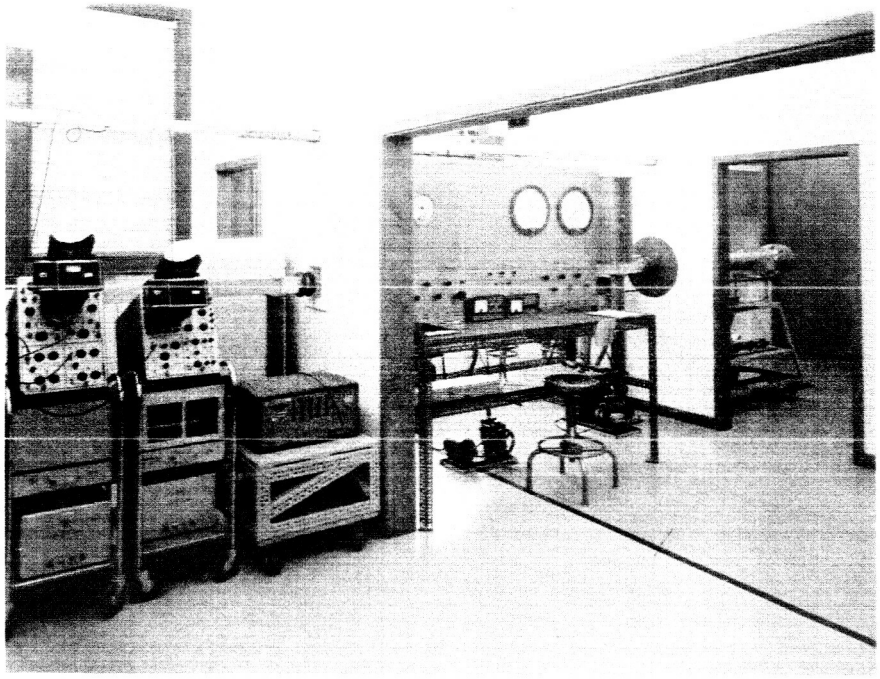

FIGURE 4. Shock Tube and Associated Equipment

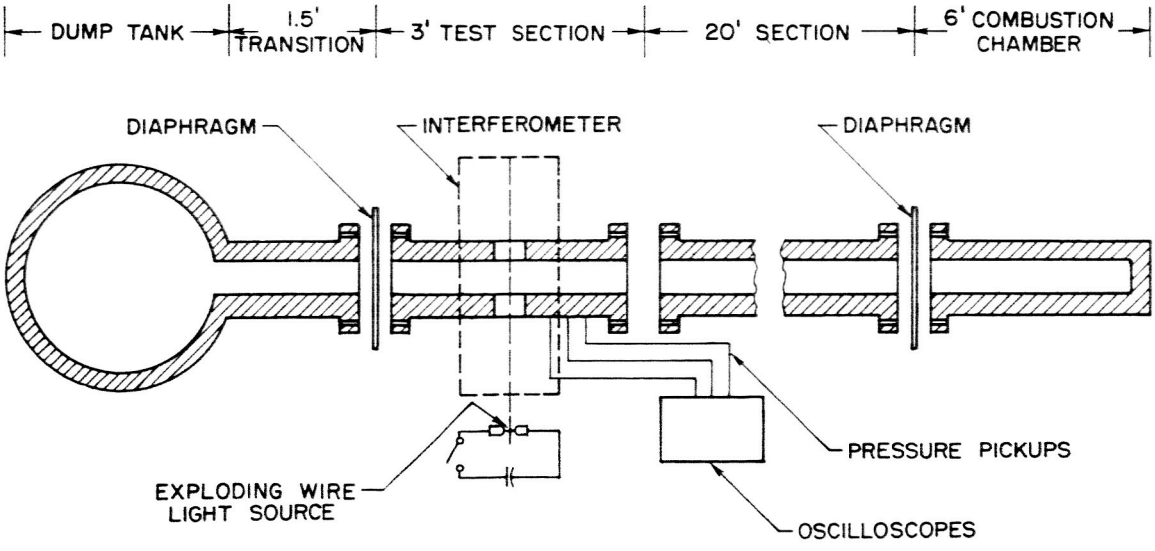

FIGURE 5. Schematic Representation of the Shock Tube and Associated Equipment

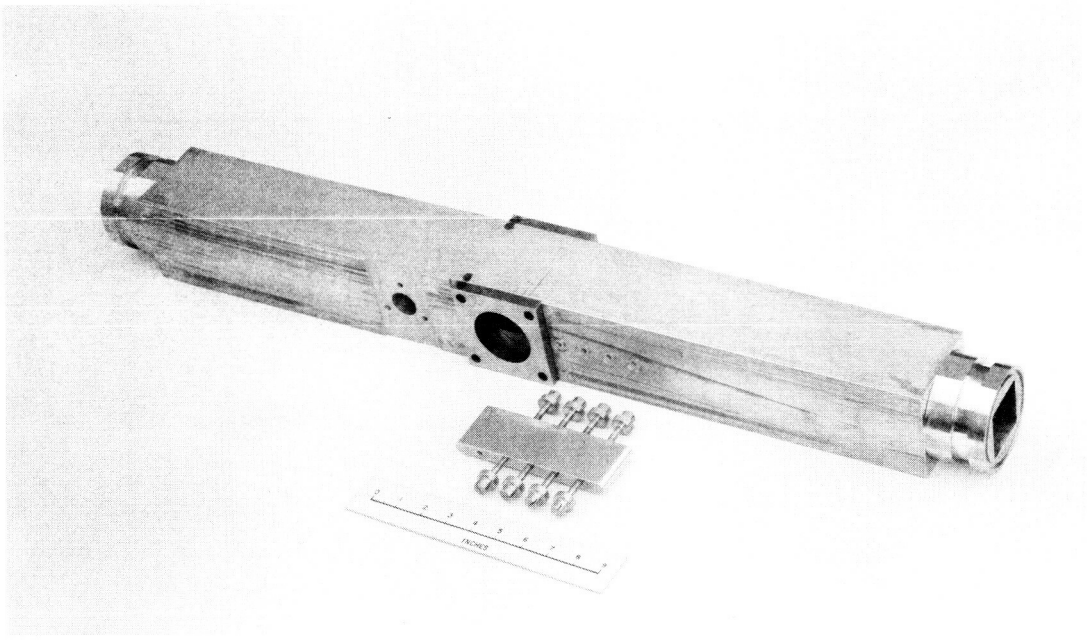

FIGURE 6. Test Section and Cylinder-Plate Model

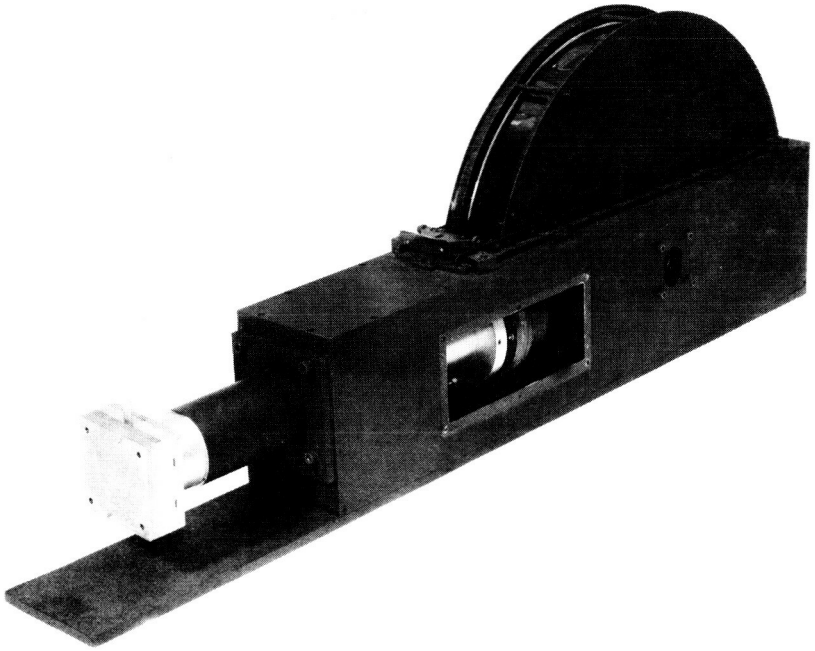

FIGURE 7. Rotating Mirror Camera

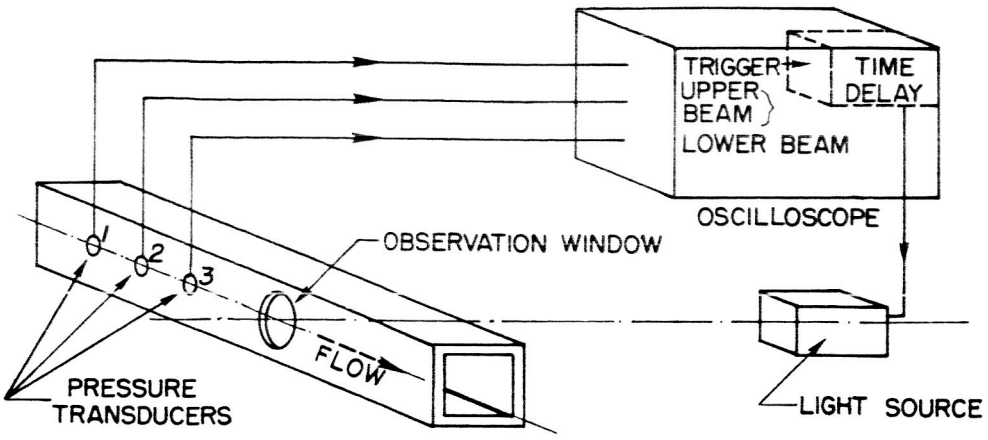

SCHEMATIC DIAGRAM OF ELECTRONIC SYSTEM

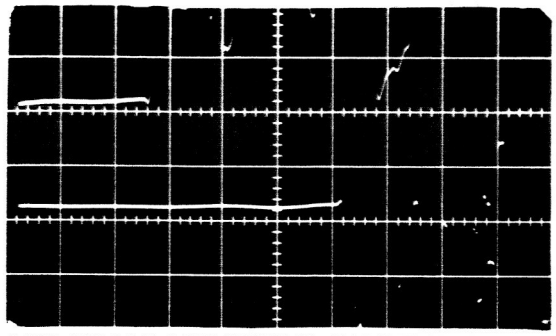

OSCILLOSCOPE TRACE MEASURING INCIDENT SHOCK VELOCITY

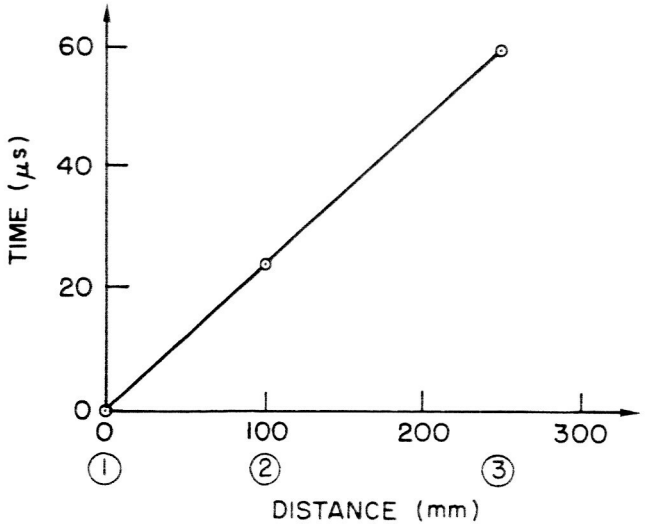

CURVE OF INCIDENT SHOCK VELOCITY

FIGURE 8. Measurement of the Shock Velocity

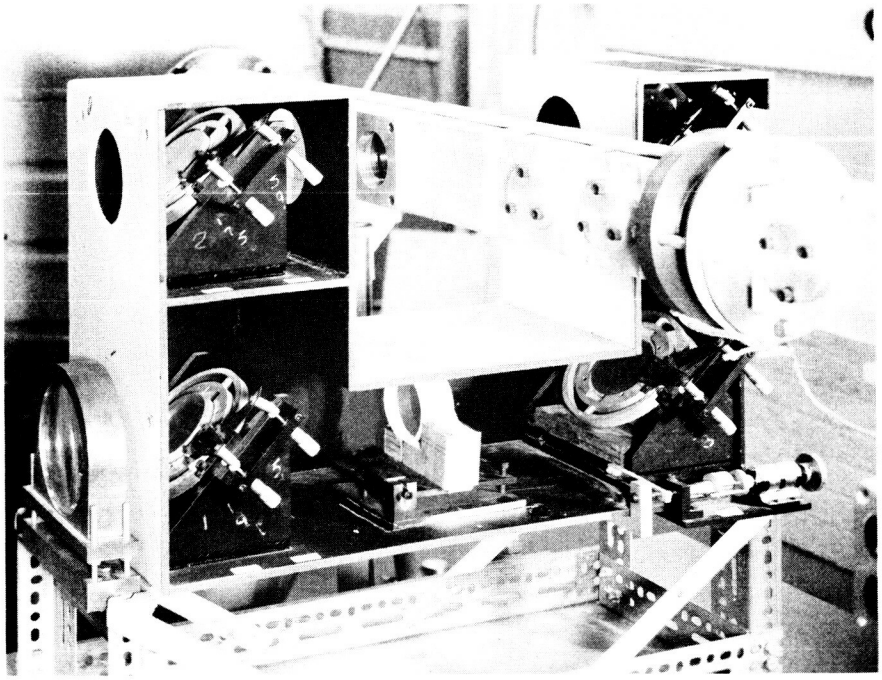

FIGURE 9. Mach-Zehnder Optical Interferometer

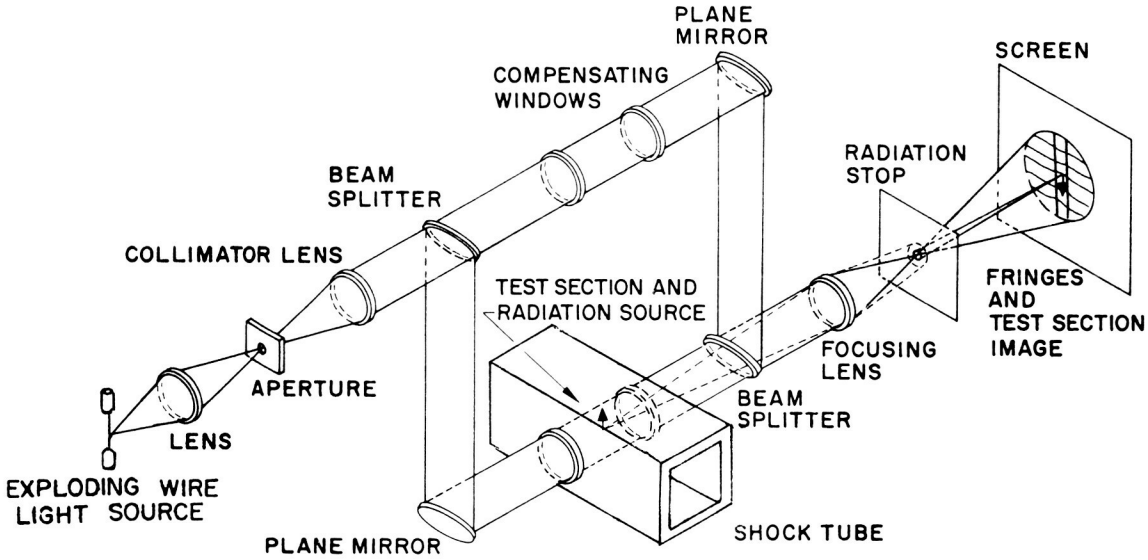

FIGURE 10. Schematic Diagram of the Optics

CHAPTER 5

EXPERIMENTAL RESULTS, COMPARISON TO THEORY, AND DISCUSSION

5.1 GENERAL CONCEPTS

Use of optical interferometry in quantitative studies of electron densities was first shown feasible by Alpher and White.[6] Measurement of both the heavy particle and electron densities is possible at any point within a plasma flow irrespective of whether the conditions at that location are in local thermal equilibrium. The dispersive nature of the electrons tends to produce a fringe shift opposite to that of the heavy particles, and becomes noticeable for electron densities of the order of 10^{17} cm^{-3}.

Since the experimental data is valid only to the accuracy to which the electronic and visual data can be recorded and reduced, it is important to determine where and to what magnitude errors in the measurements can occur. The pressure transducer-oscilloscope system enables the Mach number of the incident shock front to be determined within 1%, while measurements of fringe shifts are unlikely to exceed an accuracy of 0.1 of a fringe, dependent, of course, on the amount of photographic enlargement. Actual time readings from the time resolved rotating mirror film strips are inaccurate at less than 0.5 μsec, and the start of operation of the Kerr cell cannot be estimated to better than 1 μsec. Initial argon driven section pressures are probably

only within 0.1 mm Hg, an inaccuracy that could greatly affect low pressure tests. The cumulative effect of these errors for the incident shock tests is estimated and presented in an error "box" drawn on each plot of fringe profiles. Any experimental point on such a curve may in actuality be offset by the dimensions of the box.

The magnitude of the effect of impurities in the relaxation processes is as yet undetermined. If the pressure of the evacuated driven section, prior to each run is of the order of 10^{-5} mm Hg and is solely attributed to impurities, and if the argon gas is considered to have less than ten parts of impurities per million, then at a pressure of 5 mm Hg there would be approximately twelve parts of impurities per million parts of argon. Even if the ionization potential for such impurities is very low their inelastic collision frequency would have to be extremely large in order to produce appreciable amounts of electrons to influence the electronic relaxation length of the gas. This does not, of course, include inelastic encounters of the gas atoms with the interior surfaces of the shock tube which could produce additional ionization. Figures 16 and 17 show fringe profiles for tests wherein all conditions were equal except for the initial pressures which were 3 and 5 mm Hg respectively. In these tests it was found that the relaxation lengths could be related to each other by considering only the gas parameters without including the effects of impurities. This result implies that impurities may actually not have any appreciable effect on the relaxation length, a conclusion not generally supported by other authors.[1,4]

If impurities have little effect then the initial production of free electrons is mainly through collisions between atoms. An indirect attempt, as shown in Section 2.3.2 is made to measure the atom-atom ionization cross-section. However, due to insufficient experimental data the results are inconclusive.

In addition to evaluating the production rate of electrons by collisions between atoms, it is necessary to determine the mean energy given, by such encounters, to the resultant free electrons. For the conditions of this investigation the initial temperature of the electrons was taken to be within one-third to two-thirds of its value at the end of the relaxation zone. However, as noted in Section 2.4.1.5, for strong shocks there may actually be little variation of this temperature throughout the entire relaxation zone.

A number of effects within the flow have been neglected, such as the influence on the gas of precursor radiation, electronic diffusion, viscosity, radiation pressure, radiation enthalpy, and volume forces. The precursor radiation for the conditions of this study is estimated by Wong[4] to give degrees of ionization less than 10^{-12} and therefore has negligible effect on the flow close to the incident shock front. Near the end of the relaxation zone, however, such radiation may exert a greater influence, though such an effect was not measured in the experiments. Electron diffusion upstream through the incident shock front has been neglected due to the low electron densities behind the front and the strong Coulombic interaction between charged particles. However, the larger electron densities and temperatures in the shock layer preceding the cylinder-plate mode may produce significant electron

diffusion as well as precursor radiation through the bow wave. The result would be a thin heavy particle shock front imbedded within a wider electronic, or thermal, region as postulabe by authors such as Jaffrin.[26] However, possibly due to the insensitivity of optical interferometry to electron densities below 10^{17} cm^{-3}, such thermal regions were not experimentally observed. Viscosity, radiation pressure, radiation enthalpy, and volume forces could safely be neglected under the experimental conditions of this study.

In line with the postulated atomic model multiply excited or ionized atoms and ions were considered to exist in such small quantities to have negligible effect on the flow. However, under higher temperatures or pressures than considered here such effects might become significant and would have to be included.

Autoionization will also affect the rate of electron production. However, for the argon atom the energy difference between the two series limits is small and this phenomenon was assumed to have a negligible effect.

Lowering of the ionization potential due to the electric microfields between charged particles, and the series truncation of the partition functions have been discussed previously in Section 1.3. As with autoionization these involve complicated processes requiring further investigation. The theoretical formulation indicates, however, that a small variation in the amount of lowering of the ionization limit does affect the fringe profile sufficiently to enable experimental detection, thereby suggesting shock tube optical interferometry as a possible method for measuring this phenomenon.

The theoretical estimation of the radiated energy loss from the flow was based on the results of Horn.[7] His treatment shows that for bremsstrahlung and free-bound transitions the gas, under the experimental conditions, is optically thin and these radiation losses can be calculated by classical or hydrogenic techniques. The gas is also optically thin for bound-bound transitions between the upper excited energy levels, which were treated either hydrogenically or by the method of Bates and Damgaard.[27] For transitions between the lower excited levels of 3d to 4s and 4p to 4s the optical thickness of the gas approximated one. Radiation from such transitions was calculated by considering the losses of a unit volume located at the center of a sphere of gas having a radius of one inch and at uniform conditions. Horn actually analysed a number of geometrically different models besides the sphere, including a spatially infinite shock front, where conditions were uniform within planes parallel to the front. Since the transitions in question involved small radiation losses in all these models the overall losses from the gas were essentially the same regardless of which geometrical configuration was chosen. For the resonance transitions where the gas was optically thick and the energy of transition was large the spherical model was used.

5.2 RELAXATION AND QUASI-EQUILIBRIUM REGIONS BEHIND THE INCIDENT SHOCK FRONT

Experimental time resolved interferograms of the relaxation and quasi-equilibrium regions behind the incident shock front are shown in Figs. 11, 12, 13 and 14. These measurements are plotted on the

corresponding theoretically derived fringe profiles, numerically calculated on a Burroughs 5500 digital computer, and shown in Figs. 15, 16, 17 and 18. Shortening of the relaxation length, due to tripeling the atom-atom inelastic collision rate, is shown in Fig. 16. Note that such variations tend to change the length of the relaxation zone but not the shape of the fringe profile.

In all the experimental runs the fringes jumped in an upward direction through the incident shock front. This displacement corresponded to a change in flow conditions which could be calculated from the Rankine-Hugoniot relations. Atom-atom inelastic collisions then began producing free electrons which acquired thermal energy through elastic and superelastic (collisional de-excitation) encounters with heavy particles. After a substantial supply of such electrons was available to give a degree of ionization of the order of 10^{-3}, the computational results showed that inelastic encounters between these electrons and atoms became the dominant ionization process. For strong shocks this changeover occurred within a few millimeters behind the shock front. As the electron density increased, the dispersive nature of the electrons began shifting the fringes in a downward direction until at the end of the relaxation zone they had attained a minimum position in close agreement with the equilibrium Saha prediction. Past this location the strongly radiating flow retained essentially equal heavy particle and electron temperatures and travelled through a quasi-equilibrium region dominated by recombination processes.

In Figs. 19, 20, 21 and 22 the theoretical and experimental degrees of ionization within the relaxation and quasi-equilibrium

regions are given for incident shock Mach numbers of 18.0 into an initial pressure of 3 mm Hg, 16.3 into 3 mm Hg, 16.3 into 5 mm Hg, and 14.96 into 5 mm Hg. Note how little ionization occurs prior to the end of the relaxation zone. Figures 23 through 27 show normalized curves of mass and electron densities as well as gas pressure, particle temperatures, and emitted radiation profiles for the incident shock Mach number 18.0 test. Note that the density ratio rises from its perfect gas value of nearly four behind the shock front to above eight at the end of the relaxation zone, and then continues to increase in the quasi-equilibrium region. Also note in Fig. 27 that relatively little radiation is emitted by the flow until it reaches the end of the relaxation zone, where such emission becomes appreciable.

In calculating the amount by which the ionization potential was lowered at each point within the flow, the Ecker-Weizel polarization theory, as outlined by Pomerantz,[5] was used and resulted in lowerings of approximately 0.15 ev at the end of the relaxation zone, as shown in Fig. 28. The Inglis-Teller theory predicted lowerings of approximately 0.35 ev at this same location. This difference produced substantial enough variations in the theoretically computed fringe patterns to be observable experimentally. The results favored the polarization theory and suggested that shock tube studies might have possibilities in analysing this phenomenon.

5.3 THE SHOCK LAYER PRECEDING THE CYLINDER-PLATE MODEL

Polaroid interferograms of the shock layer preceding the cylinder-plate model for various incident shock strengths and at

various distances behind the incident front are shown in Figs. 29 through 34. Schematically the flow over the model is represented in Fig. 35. A total of twenty-three good shock layer interferograms were obtained of which these six photographs, covering the entire range of incident shock strengths investigated, are a representative sample. A number of the tests were conducted at approximately the same conditions and yielded similar fringe profiles, thereby assuring repeatability of results. Five of these six interferograms will be discussed qualitatively while the sixth, shown in Fig. 32, which was used to check the validity of the theoretical study described in Chapter 3, will be analyzed quantitatively. In all these experimental runs the initial pressure of the quiescent argon gas was 5 mm Hg and the exposure time of the interferogram was approximately 3 μsec.

The interferogram shown in Fig. 29, for an incident shock Mach number of 13.57, was taken with a 5890Å filter. The bow wave is seen a few millimeters downstream of the end of the relaxation zone behind the incident shock front. Consequently, the incoming flow into the shock layer preceding the model is in quasi-equilibrium with a calculated degree of ionization above 0.05 and an electron density of the order of 10^{16} cm^{-3}. Using the fringe shift equation derived in Section 4.1 and assuming that the degree of ionization remains constant through the shock front, the fringe shift is found to become negative (downward) at a degree of ionization of approximately 0.07. Consequently, the ionization in this experimental run must be above 0.07 and the usual upward fringe shift, due to the increase in mass density through the shock front, is suppressed by the dispersive nature of the

electrons which causes the fringes to dip downward. This negative shift continues through approximately one-third of the standoff distance of the bow wave, indicating a region wherein an increasing number of electrons are produced, until a maximum is reached at the minimum fringe position. From there up to the model's surface recombination processes dominate, accompanied by intense radiation.

The interferogram shown in Fig. 30, for an incident shock Mach number of 12.58, was split into wavelengths of 5890Å (top) and 4500Å (bottom). The bow wave is within the electronic relaxation zone behind the incident shock front and the degree of ionization of the flow entering the bow wave is quite small. Therefore, an electronic relaxation zone, extending through two-thirds of the bow wave's standoff distance, appears within the shock layer. Extreme radiation, signifying large electron concentrations is noticeable throughout a region beginning just prior to the end of the shock layer's relaxation zone and extending through the recombination dominated region up to the surface of the model.

Figure 31, at an incident shock Mach number of 12.07, is an interferogram taken with a 5890Å filter. The bow wave is well within the relaxation zone behind the incident shock front and the incoming flow is calculated to be at a Mach number of 1.38, with a degree of ionization of 0.00336, and an electron density of 2.19 (10^{15}) cm^{-3}. In this test the relaxation length within the shock layer extends through one-half of the bow wave's standoff distance. As in the previous interferograms extreme radiation is visible downstream of the end of the relaxation zone and up to the surface of the model.

Considering the standoff distance of the bow wave, the relaxation length within the shock layer, and the conditions of the incoming flow into the bow wave, this test, which was repeated and produced identical results, is not consistent with that shown in Fig. 30, a discrepancy which has not been resolved and remains as the only qualitatively unanswered phenomenon in the series of experiments.

The interferograms pictured in Fig. 32, for an incident shock Mach number of 11.32, has a split wavelength field of 5890 $\mathring{A}$ (top) and 4500 $\mathring{A}$ (bottom). This test was used to evaluate the validity of the theoretical work developed in Chapter 3. The centerline of the bow wave is 11.5 centimeters downstream of the incident shock front, and well within its relaxation zone, and the ratio of standoff distance of the bow wave to the nose radius of the model is 1.125. The computed conditions of the incoming flow into the bow wave are:

pressure = $1.079(10^{6})$ dynes/cm^{2}, density = $4.359(10^{-5})$ gm/cm^{3},

velocity = $2.737(10^{5})$ cm/sec, Mach number = 1.43,

heavy particle temperature = $1.183(10^{4})$°K,

electron temperature = $1.098(10^{4})$°K, degree of ionization = 0.00525,

electron density = $3.444(10^{15})$°K

rate of radiated energy density = $1.822(10^{7})$ ergs/cm^{3}-sec.

Fringe shift measurements were made in both wavelengths near the stagnation streamline at the following locations: across the bow wave, halfway through the relaxation zone, at the end of the relaxation zone, at the surface of the model. Since the fringe profiles are seen to vary slowly, near the bow shock's centerline, in the direction

perpendicular to the flow, these measurements were assumed to hold at the stagnation streamline and enabled the mass and electron densities and the degree of ionization to be calculated there. The results, normalized to their values just upstream of the bow wave, are shown in Fig. 36. Solid lines have been drawn through the experimental data to show the expected trends. Note that the normalized degree of ionization across the bow wave is not equal to unity as anticipated. However, this discrepancy is within the experimental reading error of the fringe shifts on the polaroid interferogram, and does not enable any conclusions to be drawn concerning the amount of electron production through the bow shock front. As in the electronic relaxation behind the incident shock fronts, there is a sharp rise in the degree of ionization and in the electron density near the end of the relaxation zone within the shock layer. A slow decrease in these quantities occurs as the surface of the model is approached. However, the mass density experiences a slow increase throughout the entire shock layer. It must be noted that since the fringe shifts are small and can be read no better than to 0.1 fringes errors in fringe measurements may be above 50%, and these results do not have the accuracy obtained for the incident shock profiles. Nevertheless, these curves are, at least, qualitatively correct.

Figure 33, for an incident shock Mach number of 10.47, shows a split wavelength interferogram, again with 5890Å (top) and 4500Å (bottom). At these slower incident shock fronts with their corresponding longer relaxation lengths the model is well within this non-equilibrium region when the interferogram was taken. Theoretical calculations show that the flow entering the bow wave has a degree of

ionization of the order of 10^{-4} and an electron density of the order of 10^{14} cm^{-3}. These low values result in a long relaxation zone within the shock layer preceding the model, extending through approximately nine-tenths of the standoff distance of the bow wave. Comparatively little radiation is noticeable near the surface of the model.

In Fig. 34, where the incident shock Mach number is 10.12, the interferogram is again split into wavelengths of 5890Å at the top and 4500Å at the bottom. As the incident Mach number of the shock decreases to this value the flow approaches that of a perfect gas with exceedingly long relaxation lengths. The bow wave is also weak and, for the short exposure times of the polaroid film, the flow within the shock layer appears to have little ionization and no visible radiation.

In comparing the results of the interferogram in Fig. 32 to those obtained from an analysis based on Chapter 3 and applicable near the stagnation line, the following conclusions were drawn.

1) A one-dimensional, time-independent solution resulted in an electronic relaxation length behind the bow wave far in excess of that measured experimentally. Though the shock layer flow is neither one-dimensional, nor time-independent, the latter condition is most likely approached within the slowly varying portions of the relaxation and quasi-equilibrium regions behind the incident shock front. However, if the shock layer is to be evaluated when the incoming flow into the bow wave emanates from the end of the relaxation zone the flow must be treated as time-dependent. Assuming a small probability for such occurrence in any experimental run future investigations may find it

wise to retain a time-independent formulation, but consider a spatially two-dimensional set of relations. The resultant partial differential equations could be reduced to ordinary differential relations by expanding the dependent parameters in terms of known functions of one of the independent variables and unknown functions of the other. Such an approach was used by Conti[28] for a reacting, non-radiating blunt body flow. Care must be exercised in the selection of the appropriate functional expansion in order to guarantee quick convergence of the series.

2) A time-dependent constant density solution yielded a physically invalid flow wherein the gas velocity increased as the particles approached the stagnation point.

Consequently, the flow near the stagnation line can neither be treated by one-dimensional methods, nor approximated by a constant density gas.

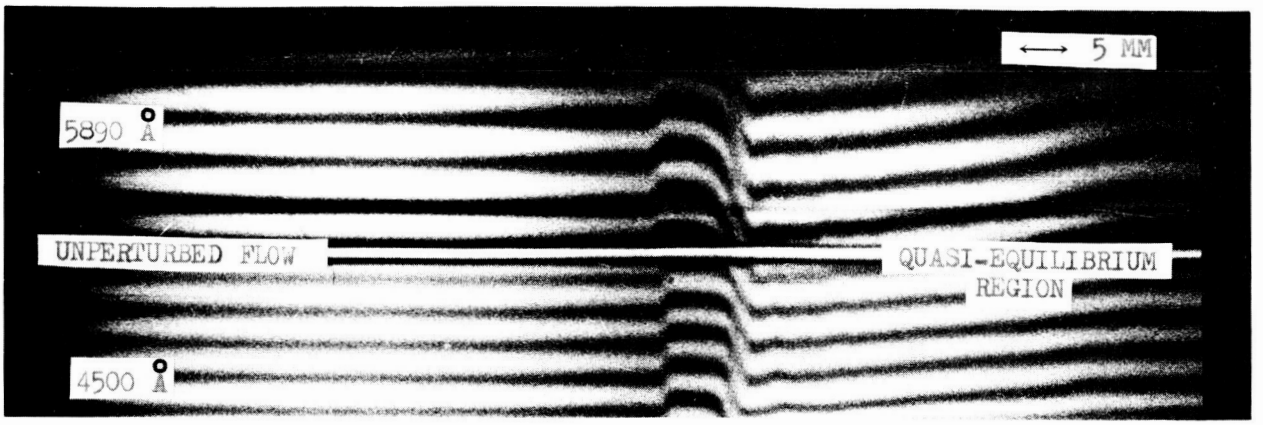

FIGURE 11. Interferogram of Mach Number 18.0 Incident Shock Front (3mm Hg)

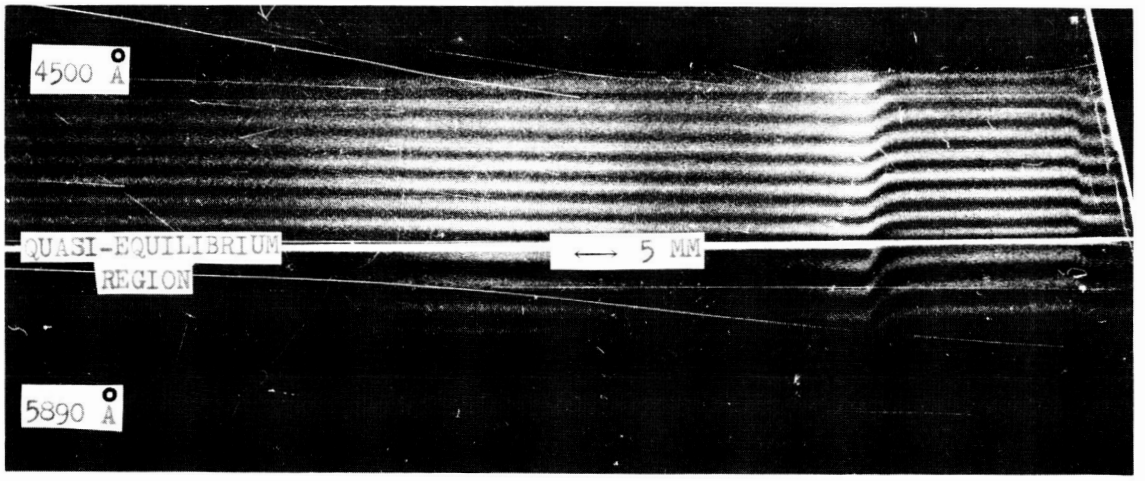

FIGURE 12. Interferogram of Mach Number 16.3 Incident Shock Front (3mm Hg)

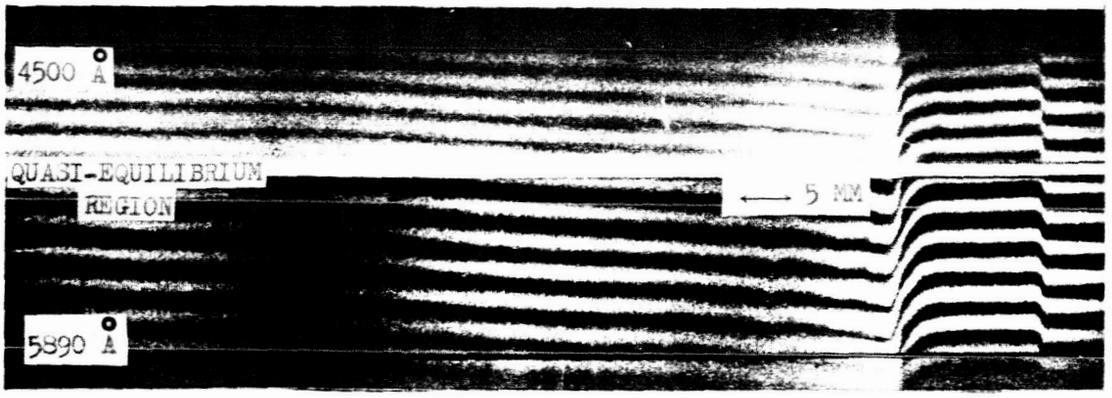

FIGURE 13. Interferogram of Mach Number 16.3 Incident Shock Front (5mm Hg)

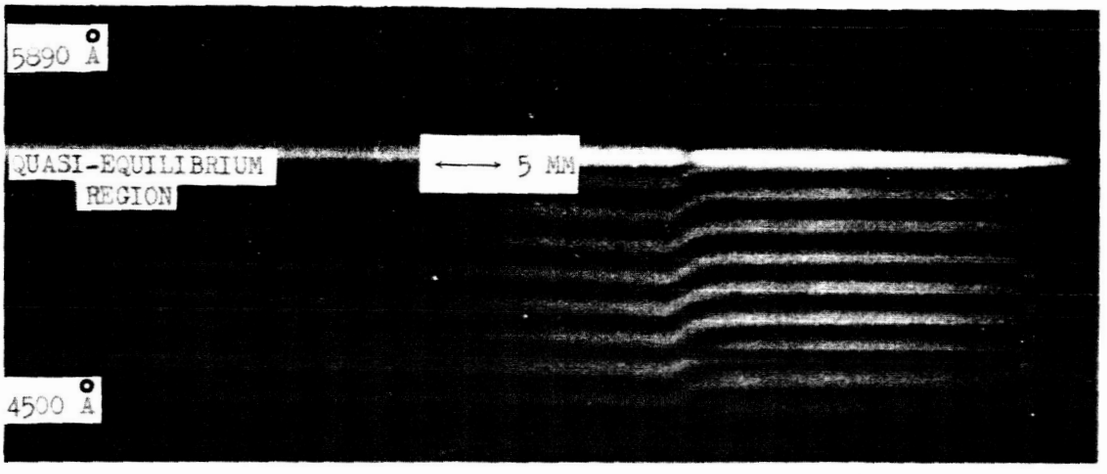

FIGURE 14. Interferogram of Mach Number 14.96 Incident Shock Front (5mm Hg)

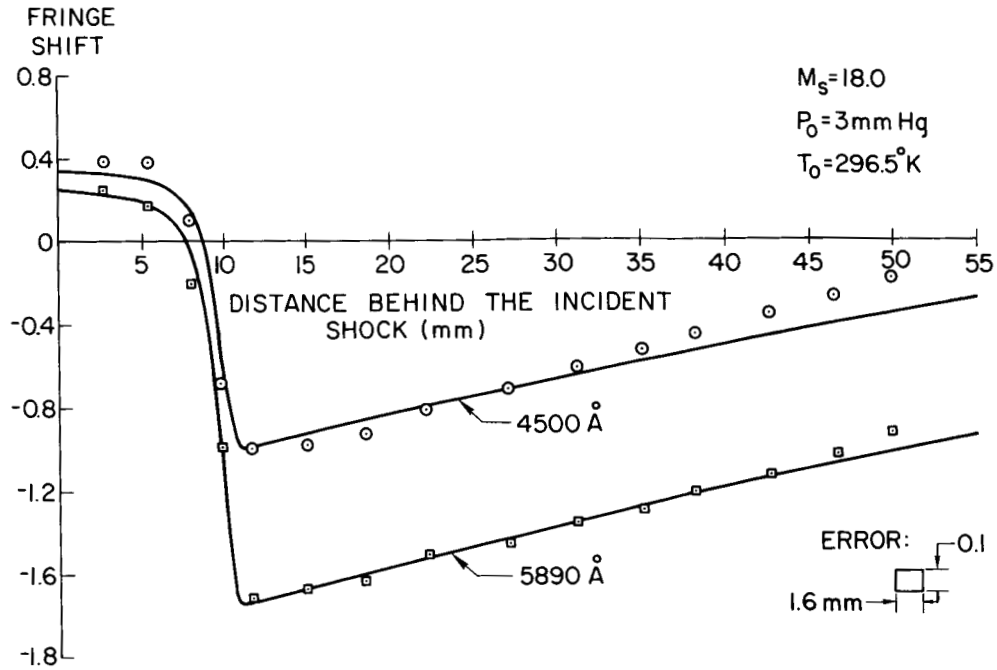

FIGURE 15. Fringe Shift Behind Mach Number 18.0 Incident Shock Front (3mm Hg)

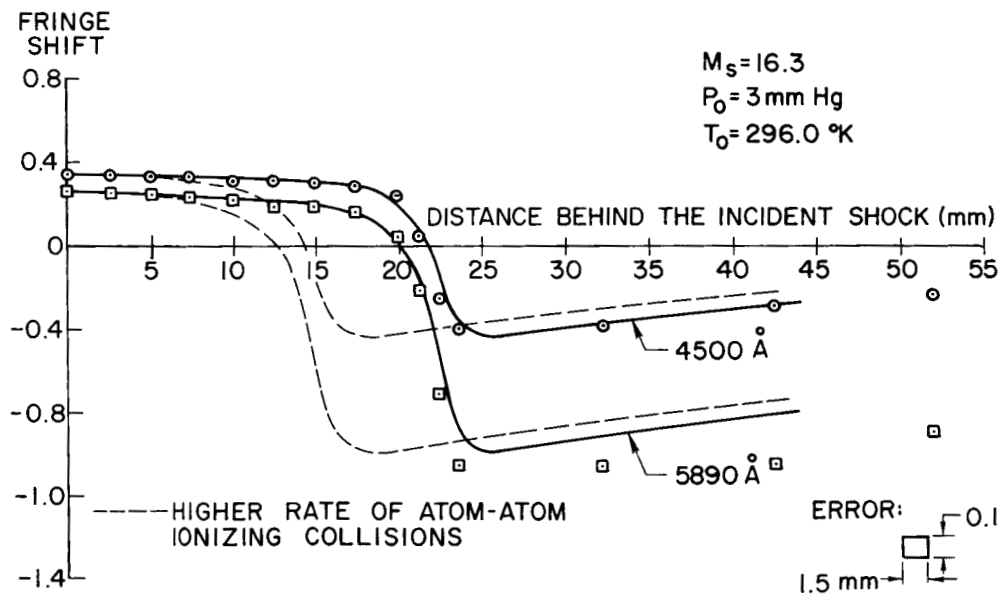

FIGURE 16. Fringe Shift Behind Mach Number 16.3 Incident Shock Front (3mm Hg)

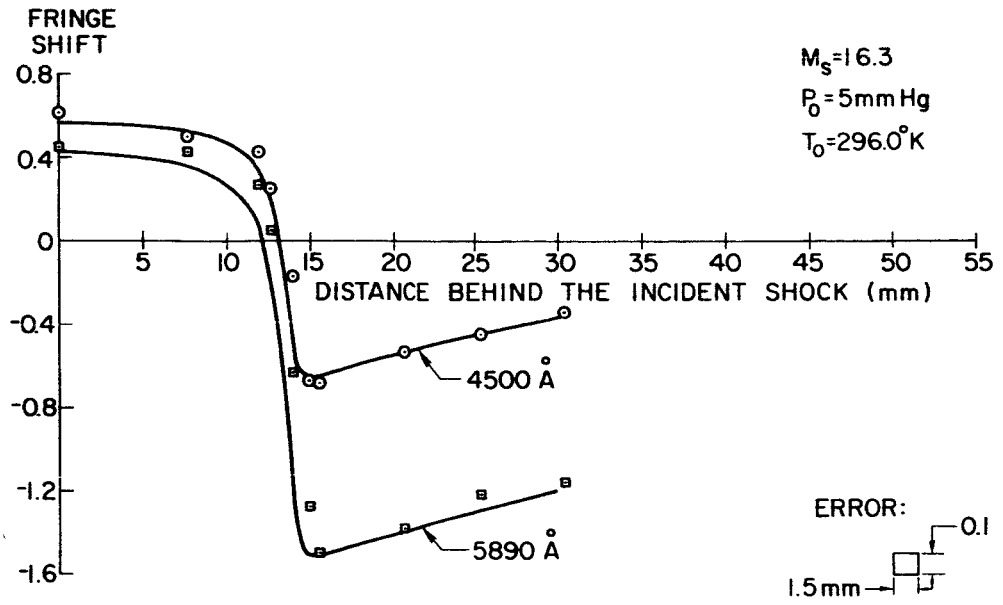

FIGURE 17. Fringe Shift Behind Mach Number 16.3 Incident Shock Front (5mm Hg)

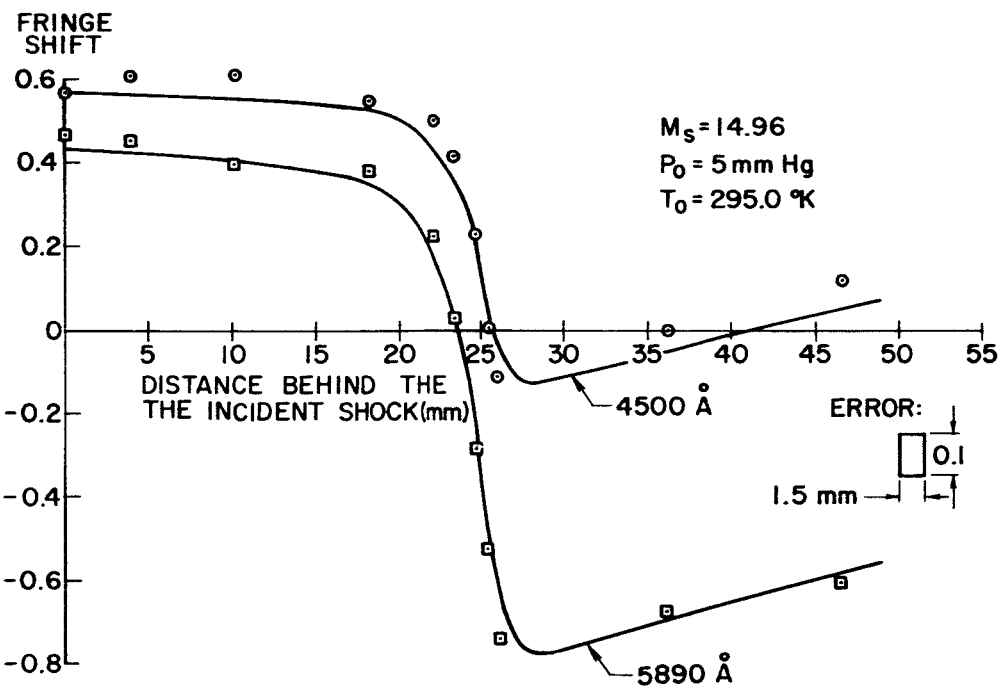

FIGURE 18. Fringe Shift Behind Mach Number 14.96 Incident Shock Front (5mm Hg)

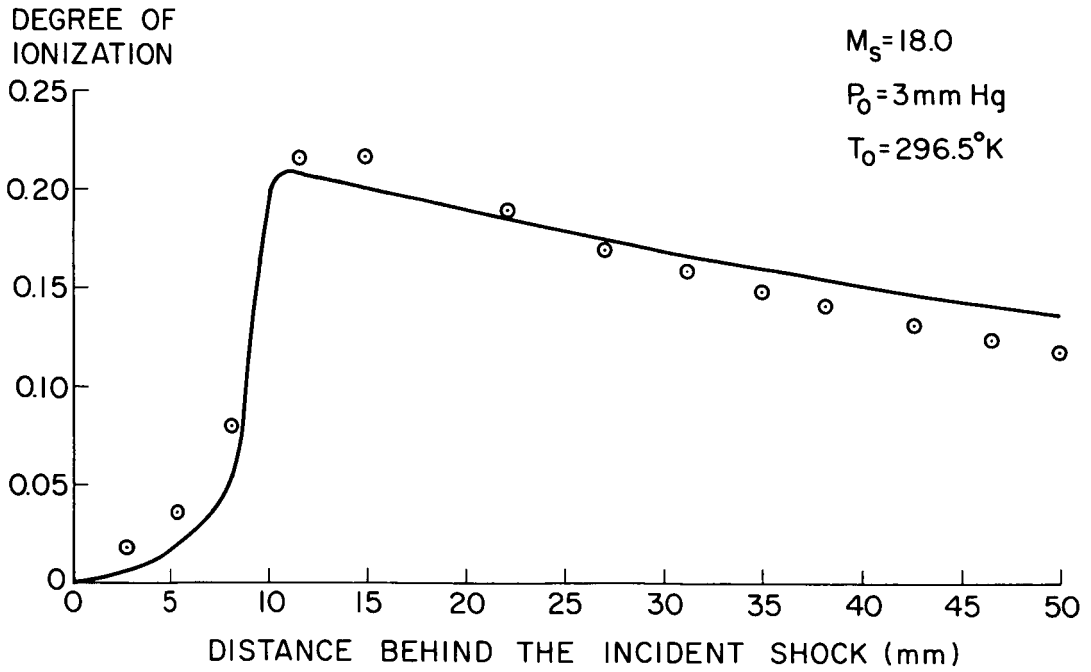

FIGURE 19. Degree of Ionization Behind Mach Number 18.0 Incident Shock Front (3mm Hg)

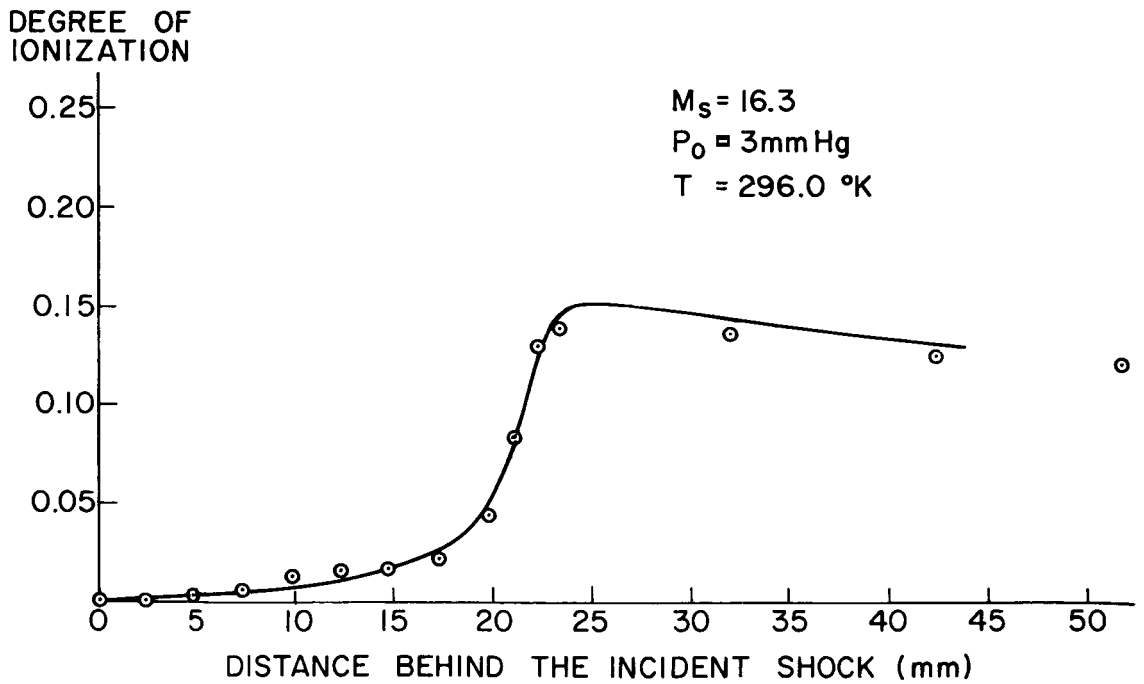

FIGURE 20. Degree of Ionization Behind Mach Number 16.3 Incident Shock Front (3mm Hg)

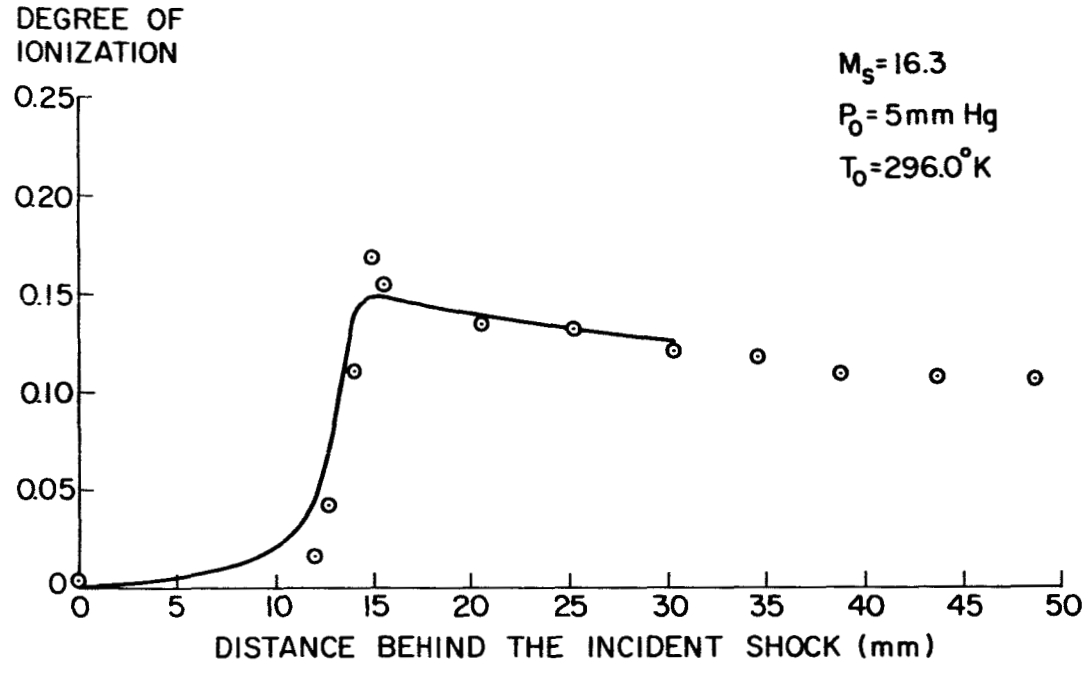

FIGURE 21. Degree of Ionization Behind Mach Number 16.3 Incident Shock Front (5mm Hg)

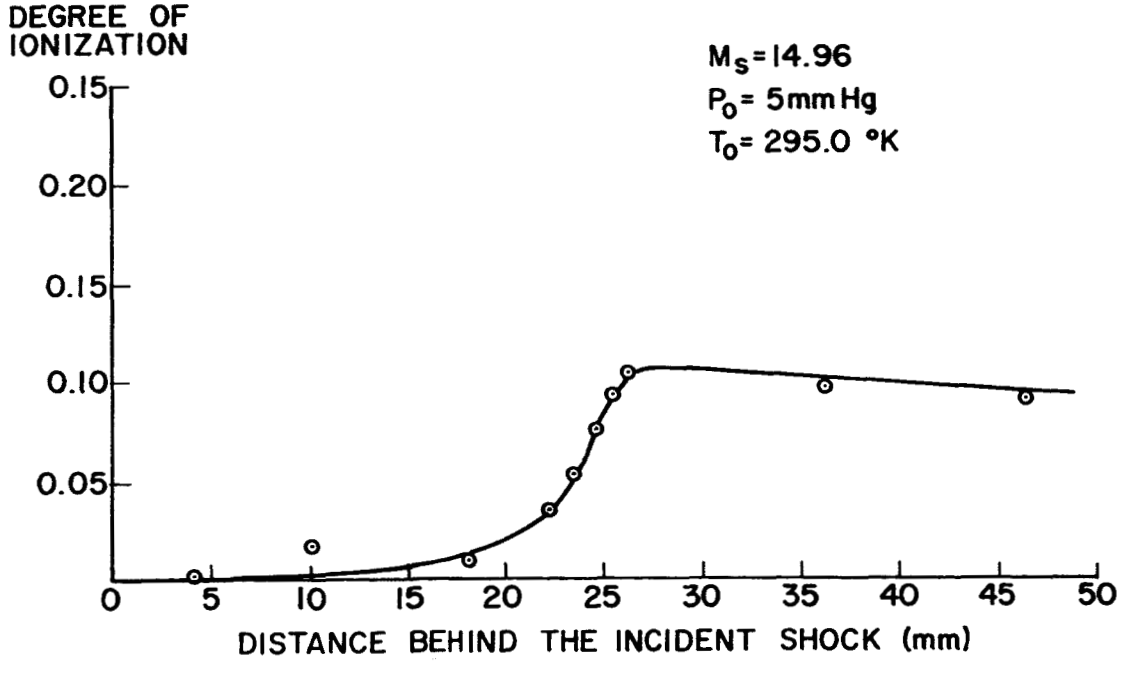

FIGURE 22. Degree of Ionization Behind Mach Number 14.96 Incident Shock Front (5mm Hg)

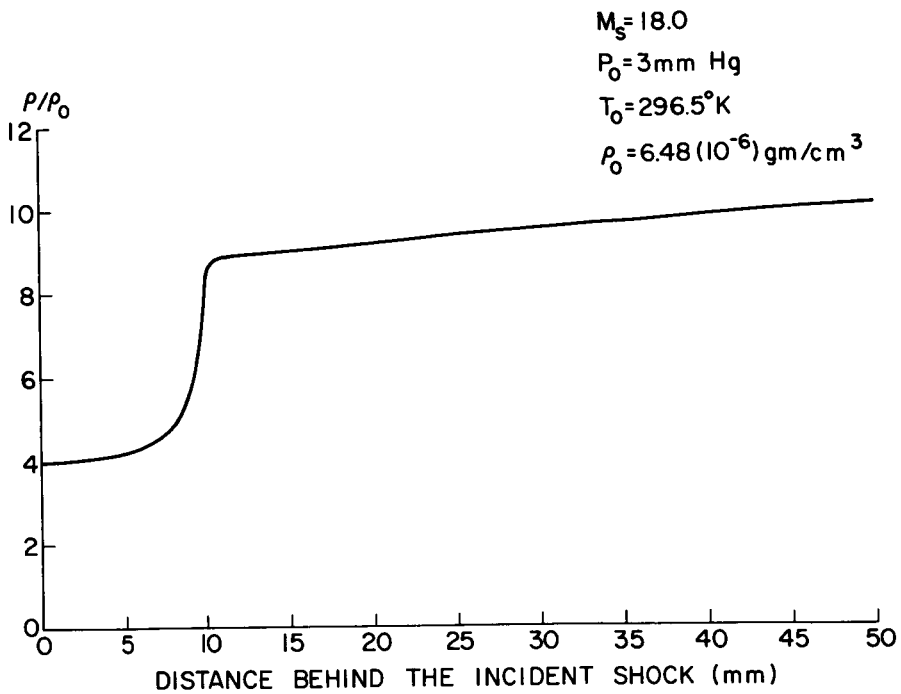

FIGURE 23. Mass Density Behind Mach Number 18.0 Incident Shock Front (3mm Hg)

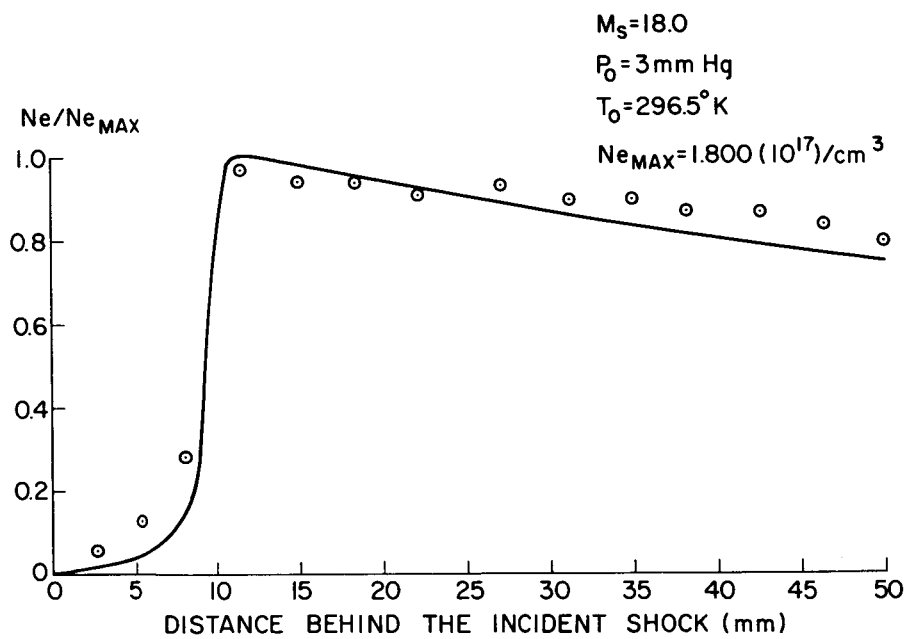

FIGURE 24. Electron Density Behind Mach Number 18.0 Incident Shock Front (3mm Hg)

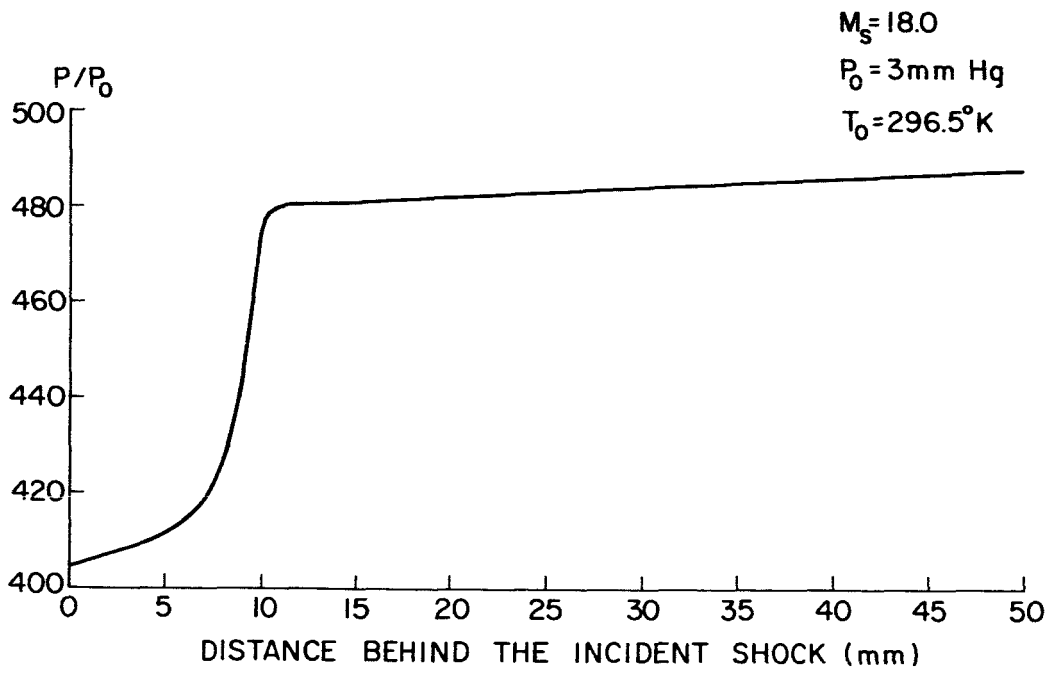

FIGURE 25. Gas Pressure Behind Mach Number 18.0 Incident Shock Front (3mm Hg)

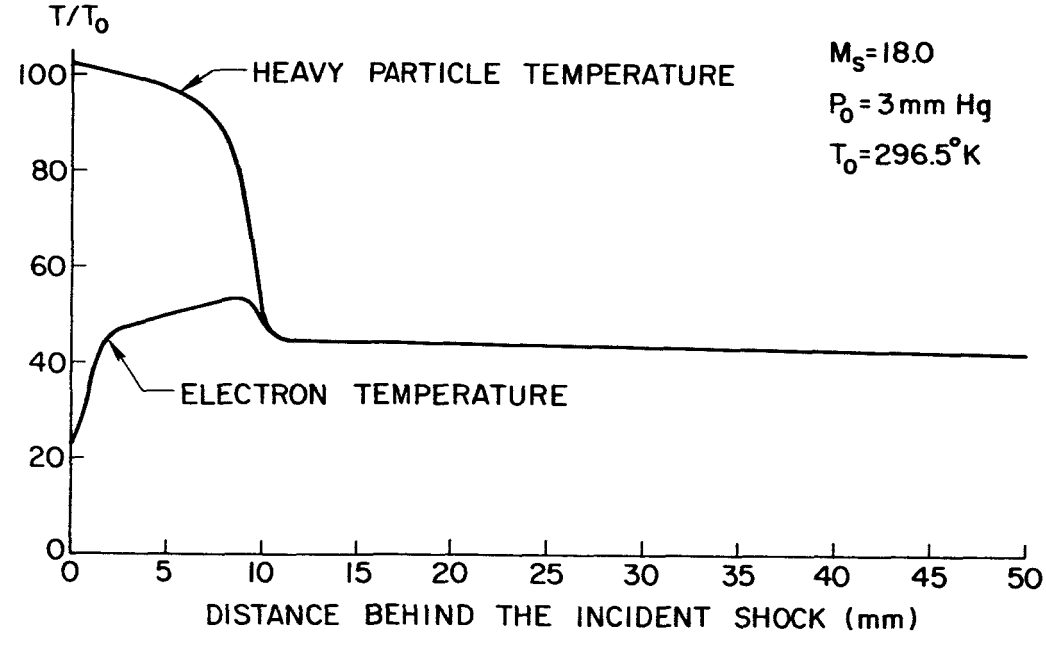

FIGURE 26. Heavy Particle and Electron Temperatures Behind Mach Number 18.0 Incident Shock Front (3mm Hg)

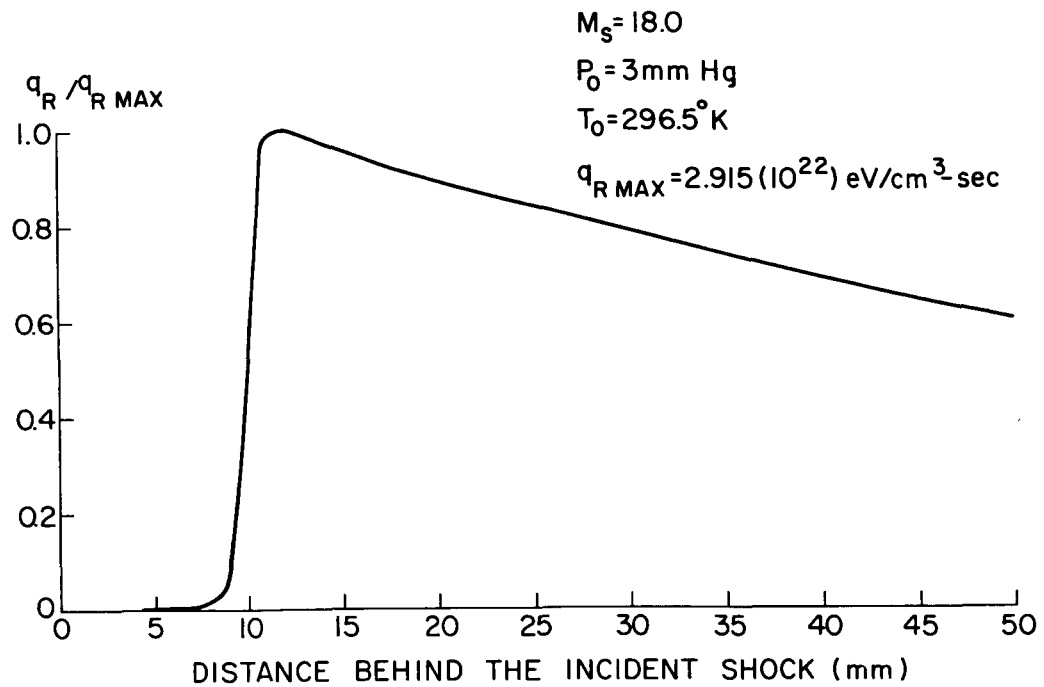

FIGURE 27. Rate of Radiative Loss Behind Mach Number 18.0 Incident Shock Front (3mm Hg)

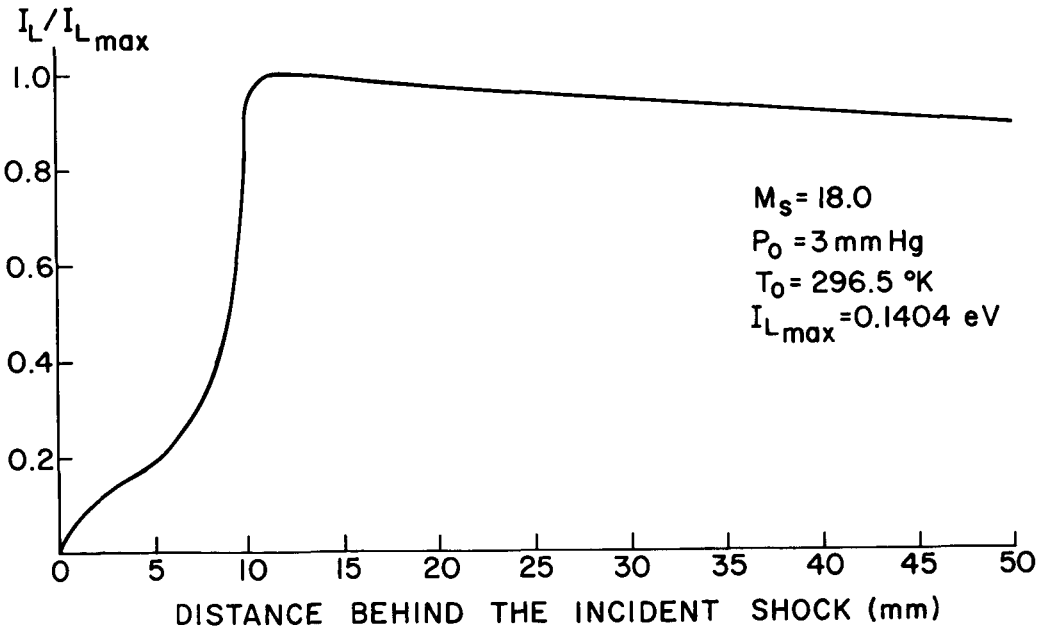

FIGURE 28. Lowering of the Ionization Potential Behind Mach Number 18.0 Incident Shock Front (3mm Hg)

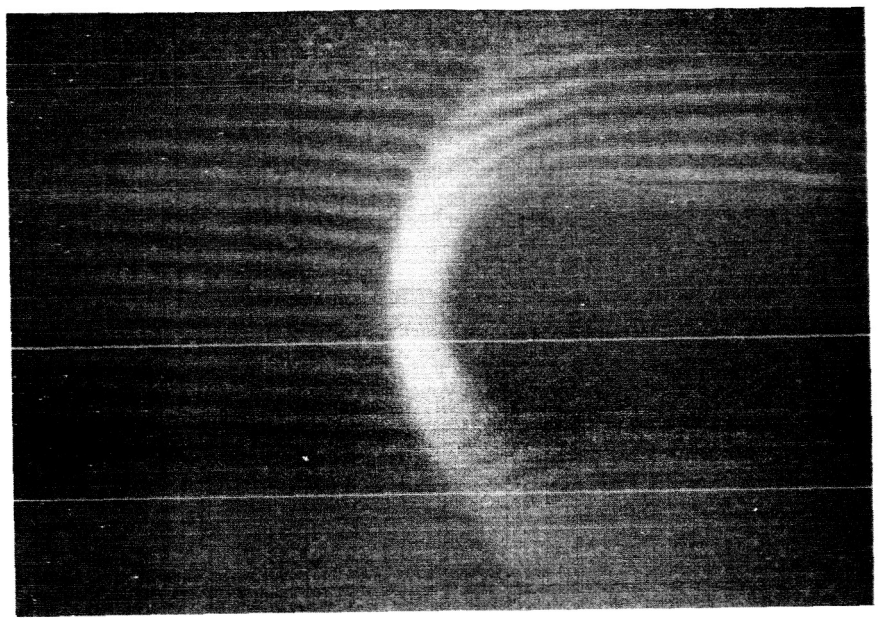

FIGURE 29. Interferogram of the Shock Layer Preceding the Cylinder-Plate (Incident Shock Mach Number 13.57)

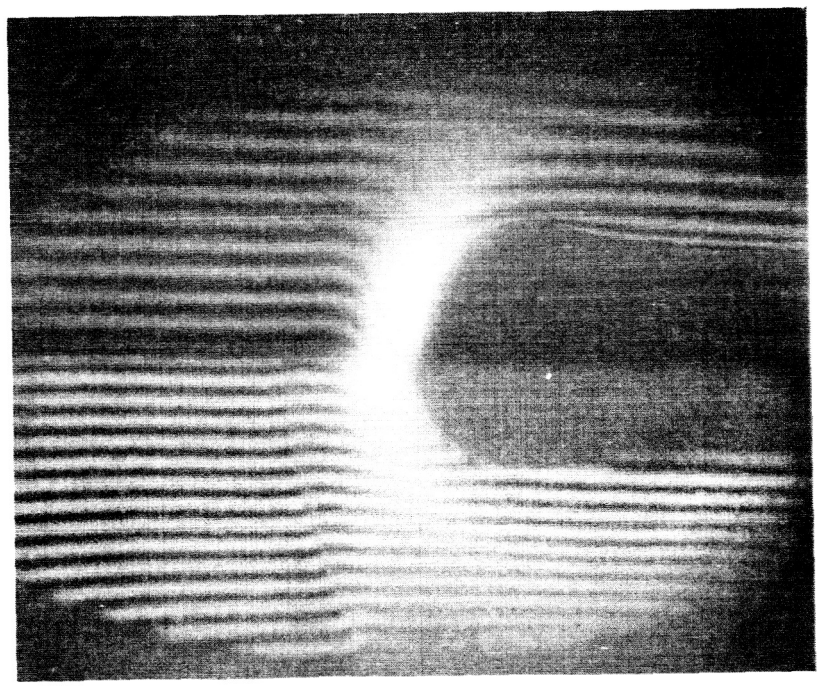

FIGURE 30. Interferogram of the Shock Layer Preceding the Cylinder-Plate (Incident Shock Mach Number 12.58)

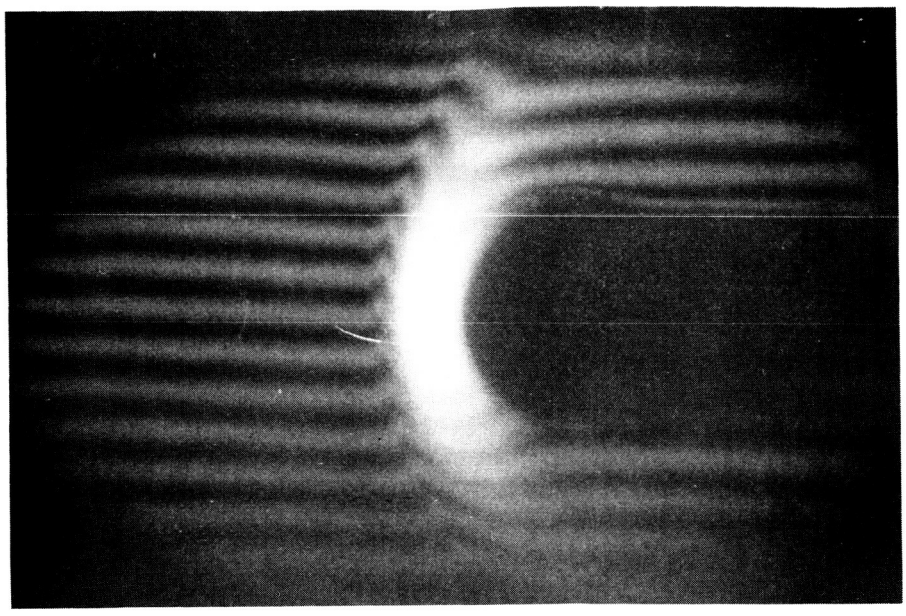

FIGURE 31. Interferogram of the Shock Layer Preceding the Cylinder-Plate (Incident Shock Mach Number 12.07)

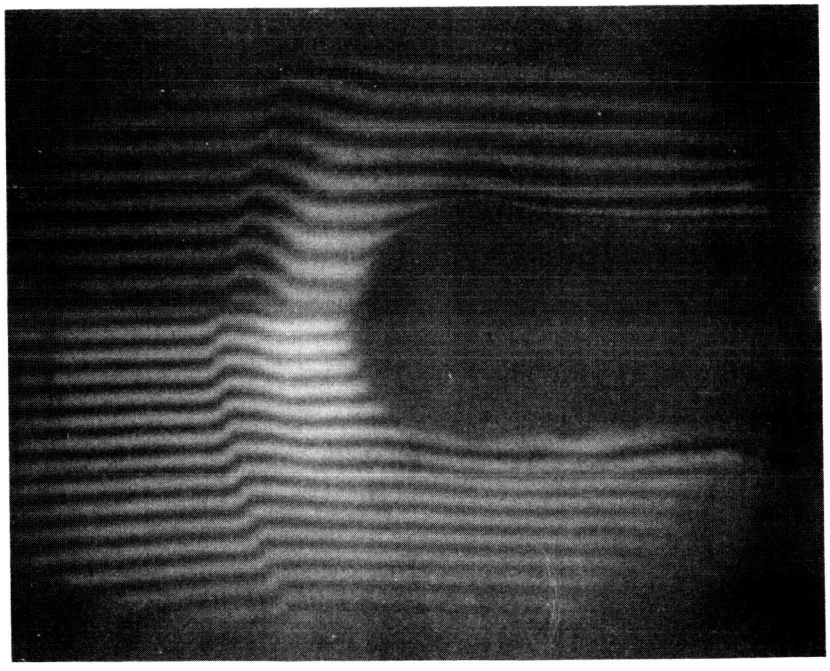

FIGURE 32. Interferogram of the Shock Layer Preceding the Cylinder-Plate (Incident Shock Mach Number 11.32)

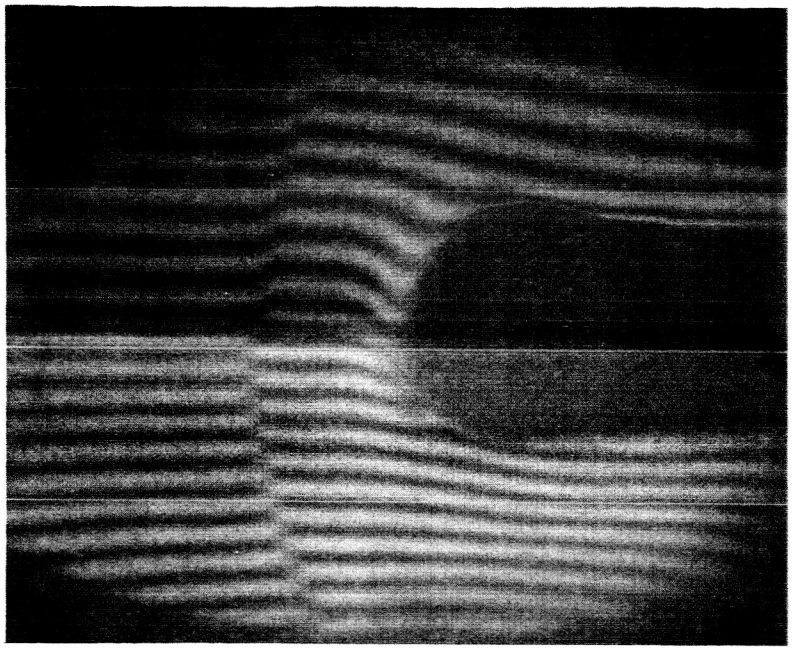

FIGURE 33. Interferogram of the Shock Layer Preceding the Cylinder-Plate (Incident Shock Mach Number 10.47)

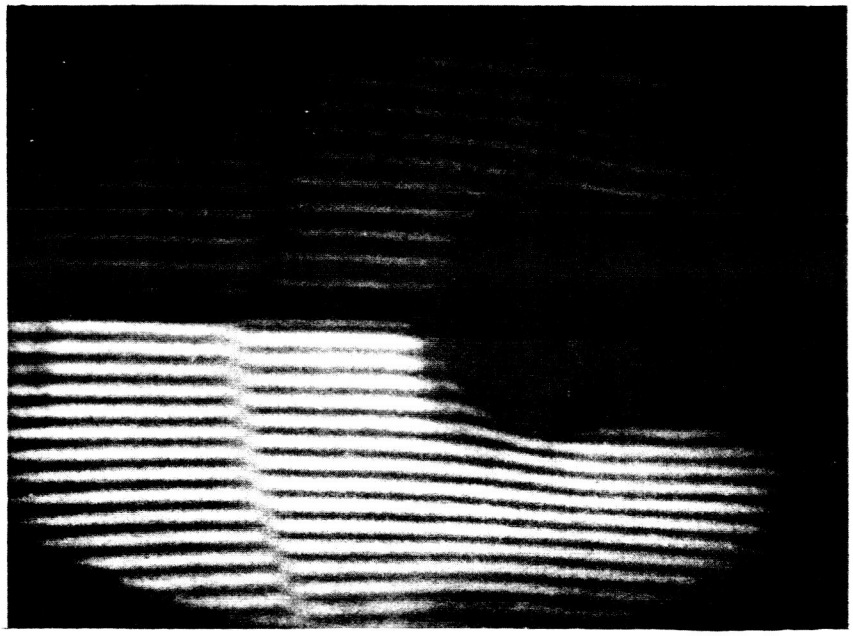

FIGURE 34. Interferogram of the Shock Layer Preceding the Cylinder-Plate (Incident Shock Mach Number 10.12)

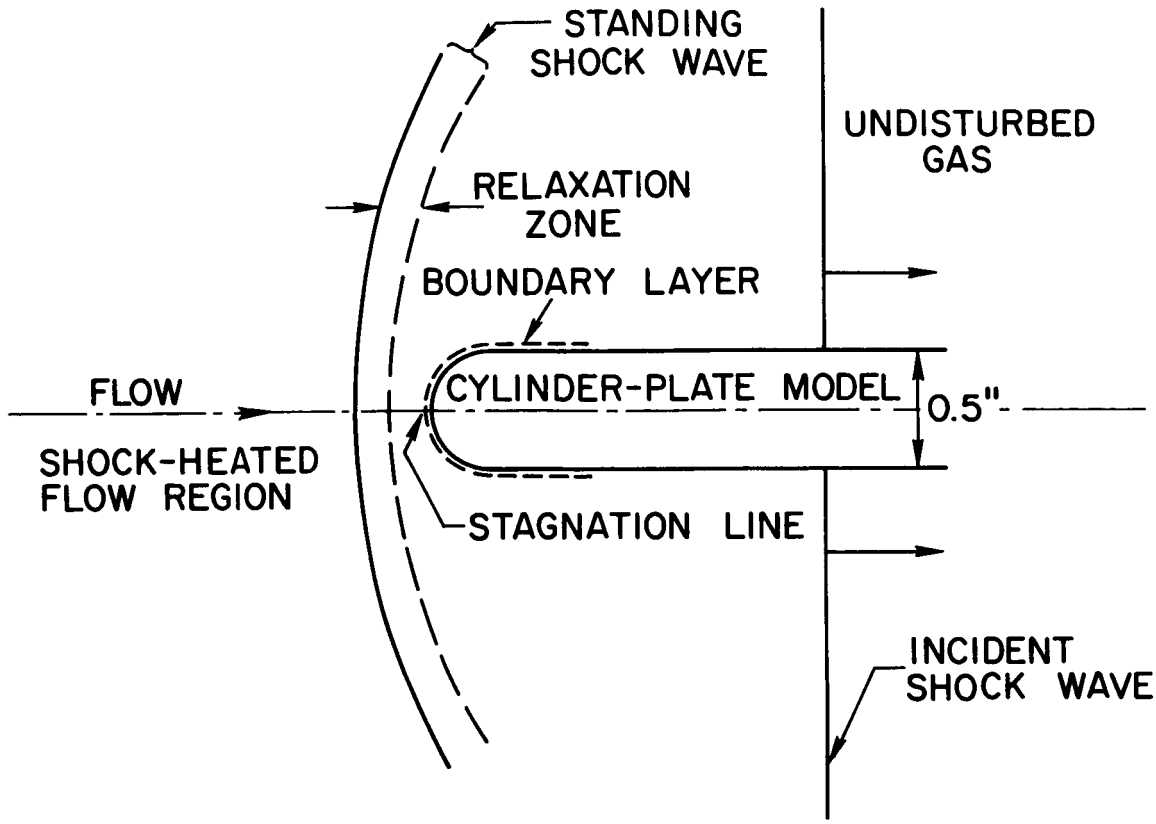

FIGURE 35. Schematic Representation of the Flow over the Cylinder-Plate

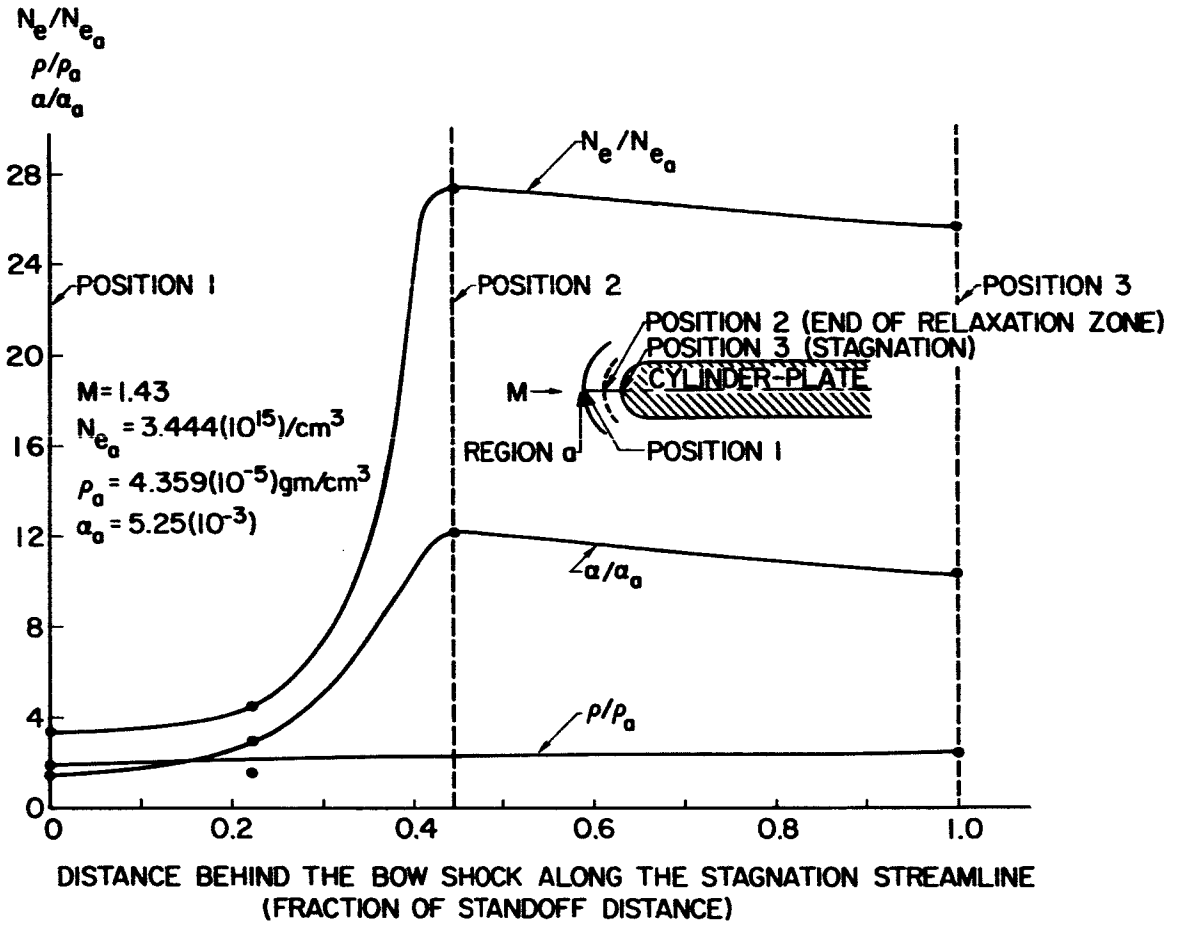

FIGURE 36. Mass and Electron Densities and Degree of Ionization Within the Shock Layer Preceding the Cylinder-Plate (Incident Shock Mach Number 11.32)

CHAPTER 6

SUMMARY AND CONCLUSIONS

The electronic relaxation phenomenon in a shock heated argon gas is a complex process requiring investigation of the microscopic collisional and radiative mechanisms within the flow. A Lagrangian mathematical formulation of such a non-equilibrium, radiating argon plasma flow consists of six relations, three of which are ordinary non-linear differential equations. These expressions include the effects of elastic and inelastic encounters between the following species: ground state atoms, excited atoms, ground state ions, and free electrons. Radiation losses are calculated by investigating the possible transitions within the atom and the optical depths of the gas associated with each one. Additional effects such as electric microfield lowering of the ionization potential and series truncation of the atomic partition function are also considered.

The time-independent, one-dimensional reduced set of relations is applied to the flow behind a strong, normal, incident shock front. Resulting fringe profiles of the electronic relaxation and quasi-equilibrium flow regions, for Mach numbers of 11 to 18 into initial argon pressures of 3 to 5 mm Hg, correlate well, for arbitrarily chosen inelastic collison rates of the atoms, with the experimental time resolved dual wavelength interferograms.

As the atoms pass through the shock front they experience a jump in conditions which obey the Rankine-Hugoniot relations. Subsequent atom-atom inelastic collisions produce the initial supply of free electrons. Since such inelastic cross-sections are not known for energies of a few electron volts, the electron production rate by this mechanism, which dominates only in the region close to the shock front, is arbitrarily chosen to correlate the theoretical relaxation length with its experimental value. Within a short distance behind the shock front, approximately one millimeter for the stronger shocks, an adequate number of free electrons are available so that electron-atom collisions dominate the ionization processes.

Relatively small changes occur in the flow variables within the relaxation zone until close to its end where conditions rapidly change. Mass and electron densities, pressure, and emitted radiation all rise sharply until, at the end of the relaxation zone, conditions agree with the Saha equilibrium prediction. Then, in the quasi-equilibrium regime, where the heavy particle and electron temperatures are equal, recombination processes dominate and the degree of ionization, electron density, gas temperature, and emitted radiation decrease slowly, while the mass density and the pressure continue to experience a steady rise.

Both the time-independent, one-dimensional, and the time-dependent Lagrangian formulations were applied along the stagnation line within the shock layer preceding the cylinder-plate model. In order to retain a set of ordinary differential equations constant

density was assumed in the Lagrangian formulation. However, neither of these theoretical treatments agreed with the experimental results, since the former produced relaxation lengths behind the bow wave far in excess of those measured experimentally, and the latter resulted in the physically invalid solution wherein the flow velocity increased as the gas particles approached the stagnation point.

Qualitative results of the experimentally obtained still Polaroid interferograms of the shock layer indicate little electronic relaxation within this layer for the higher incident shock Mach numbers above 13, when the incoming flow emanates from the quasi-equilibrium region behind the incident shock. For weaker incident shocks, below 13, the interferograms were taken while the model was within the relaxation zone behind the incident shock front. Therefore, the flow entering the bow wave had a relatively small electron density, causing within the shock layer, an electronic relaxation zone which varied in length depending on the strength of the incident shock front. The region beginning just prior to the end of the shock layer's relaxation zone and extending to the surface of the model was marked by considerable radiation for incident shock strengths above 10.5. When this Mach number decreased to approximately 10 the degree of ionization became so small as to be undetected in the fringe profiles and the interferograms appeared similar to those expected for a perfect gas flow.

APPENDIX A

DETERMINATION OF A FUNCTIONAL FORM FOR THE RADIATION DENSITY

Nicholls[11] considers a volume element $(dx)(1)$ emitting $j_\nu \frac{d\Omega}{4\pi} \rho \, dx$ into the solid angle $d\Omega$

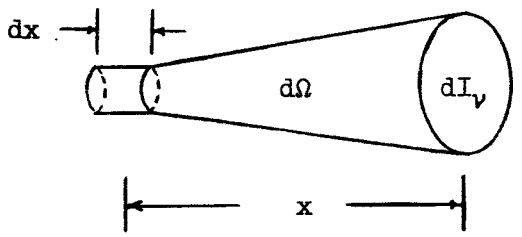

The intensity increment at x due to the emission of this volume element into $d\Omega$ is,

$$dI_\nu = j_\nu \rho \frac{d\Omega}{4\pi} dx \exp(-\kappa_\nu \rho x)$$

where κ_ν is the mass absorption coefficient. If the intensity is isentropic, i.e., independent of angle, it can be obtained by integrating the above expression, resulting in

$$I_\nu = \int_0^x dI_\nu = \frac{j_\nu}{\kappa_\nu} [1 - \exp(-\kappa_\nu \rho x)]$$

However, from Kirchoff's law, for thermal equilibrium,

$$\frac{j_\nu}{\kappa_\nu} = B_\nu(T)$$

and since the optical depth is defined as, $\tau_\nu \triangleq \kappa_\nu \rho x$ the relation denoting intensity becomes,

$$I_\nu = B_\nu(T)\ [1 - \exp(-\tau_\nu)]$$

Consider, now, a volume V with surface area δ,

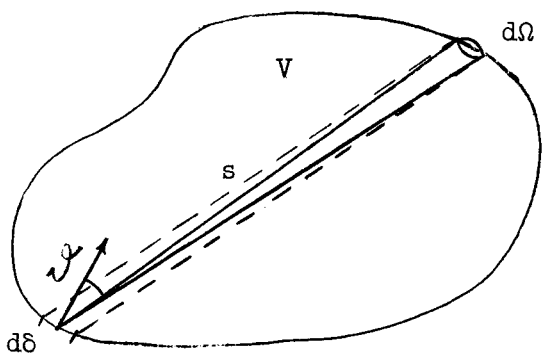

The time required for the radiation to travel the distance s is s/c. Therefore, the energy in V is,

$$V\rho_R(\nu) = \int_\Omega \int_\delta I_\nu(\vartheta,\varphi)\ d\delta\ \cos\vartheta\ d\Omega\ \frac{s}{c}$$

But, $d\delta \cos\vartheta\ s = dV$, so that $\rho_R(\nu) = \frac{1}{c}\int_\Omega I_\nu\ d\Omega$, or if the intensity is isentropic, $\rho_R(\nu) = \frac{4\pi}{c} I_\nu$.

Substituting this relation into the above expression for intensity yields,

$$\rho_R(\nu) = \frac{4\pi}{c} B_\nu(T)\ [1 - \exp(-\tau_\nu)]\ .$$

APPENDIX B

DETERMINATION OF THE VOLUME ABSORPTION COEFFICIENTS FOR THE TWO RESONANT TRANSITIONS FROM THE 4s LEVEL, AT THE RESONANT FREQUENCY

Consider the natural (Lorentz) profile of the volume absorption coefficient for stationary atoms and add to this collisional (Stark) broadening due to the electric microfields, and finally superimposes the thermal (Doppler) broadening at each frequency due to the velocity distribution of the atoms. Then, from Nicholls,[11]

$$k_\nu = \frac{k_0}{\pi(\Delta\nu_N + \Delta\nu_c)} \int_{-\infty}^{\infty} \frac{\exp[-((2\eta/\Delta\nu_D)\sqrt{\ln 2})^2]}{1 + [\frac{2}{\Delta\nu_N + \Delta\nu_c}(\nu - \nu_{0,1} - \eta)]^2} d\eta$$

where Sibulkin[29] gives,

$$k_0 = \left(\frac{m_A \pi}{2}\right)^{1/2} \frac{e^2 f_{0,1} n(0)}{m_e \nu_{0,1} (kT_e)^{1/2}}$$

and $\Delta\nu_N$, $\Delta\nu_c$, $\Delta\nu_D$ are the spectral line widths due to natural, collisional, and thermal broadening respectively. This integral must be solved numerically except at the resonant frequency where it reduces to,

$$k_{\nu_{0,1}} = k_0 \left[1 - \text{erf}\left(\frac{\Delta\nu_N + \Delta\nu_c}{\Delta\nu_D}\sqrt{\ln 2}\right)\right] \exp\left[(\ln 2)\left(\frac{\Delta\nu_N + \Delta\nu_c}{\Delta\nu_D}\right)^2\right]$$

The natural, thermal, and collisional widths can be expressed respectively as,

$$\Delta\nu_N = \frac{4\pi e^2 \nu_{0,1}^2}{m_e c^3 g(1)} g(0)\, f_{0,1}$$

$$\Delta\nu_D = \frac{2\nu_{0,1}}{c} (2RT_A \ln 2)^{1/2}$$

$$\Delta\nu_c = \Delta\nu_{c(\text{resonance broadening})} + \Delta\nu_{c(\text{quadratic Stark effect})}$$

where the Stark broadening is composed of two parts when resonance transitions are involved.

Consider the four first excited, or $3p^5 4s$, states of the atom which have quantized j values 1, 0, 1, 2. Since for allowable transitions $\Delta j = \pm 0, 1$, with $0 \rightarrow 0$ transitions excluded, only resonance transitions from the two $j = 1$ levels can occur, each level having a degeneracy, $g(1)$, of 3. Knox[12] using Hartree-Fock relations determined the oscillator strengths corresponding to these transitions, one of which is a singlet while the other is a triplet, to be,

$$^1f_{0,1} = 0.20 \qquad \text{and} \qquad ^2f_{0,1} = 0.05$$

where the wavelengths are respectively 1049 Å and 1067 Å.

The collisional width for these resonance transitions is given by Nicholls[11] as,

$$\Delta\nu_c = \frac{e^2}{8m_e\nu_{0,1}} f_{0,1}\, n(0) + \frac{38.8}{2\pi} c_s^{2/3} u_e^{1/3} n_e$$

where,[30] $C_s = 10^{-14}$ cm^4 sec^{-1} and,[31] $u_e = (8kT_e/\pi m_e)^{1/2}$.

For an atom temperature, T_A, of the order of 1 ev and an electron density, n_e, of the order of 10^{17} cm^{-3} the volume absorption coefficients at the resonant frequency for these singlet and triplet transitions respectively are calculated to be,

$$^1k_{\nu_{0,1}} = 0[2(10^4)] \text{ cm}^{-1}$$

and

$$^3k_{\nu_{0,1}} = 0[7(10^3)] \text{ cm}^{-1}$$

APPENDIX C

RELATION BETWEEN THE OSCILLATOR STRENGTH AND THE EINSTEIN $\bar{A}$ AND $\bar{B}$ COEFFICIENTS

Following the analysis of Unsöld,[32] the absorption of energy per unit time and volume in the solid angle $d\Omega$ and frequency range $d\nu$ is,

$$k_\nu I_\nu \, d\nu \, d\Omega$$

Integrating over all frequencies and, for the case of isentropic intensity, over all solid angles the absorbed energy is,

$$4\pi \, I_\nu \int k_\nu \, d\nu$$

However, in Appendix A it was shown that,

$$4\pi I_\nu = c \, \rho_R(\nu)$$

so that the energy absorbed per unit time and area at a frequency corresponding to transitions from a state q to a state p is,

$$c \, \rho_R(\nu_{q,p}) \int k_\nu \, d\nu$$

If this absorbed energy produces stimulated transitions of electrons between these two states it can be equated to the energy increase of the electrons,

$$\bar{B}(q,p)\ h\nu_{q,p}\ n(q)\ \rho_R(\nu_{q,p})$$

Therefore,

$$\int k_\nu\ d\nu = \frac{h\nu_{q,p}}{c}\ \bar{B}(q,p)\ n(q)$$

Comparing this result with the following classically derived relation,

$$\int k_\nu\ d\nu = \frac{\pi e^2}{m_e c}\ n(q)\ f_{q,p}$$

where $f_{q,p}$ denotes the oscillator strength corresponding to transitions from state q to p, enables the Einstein $\bar{B}$ coefficient to be expressed as,

$$\bar{B}(q,p) = \frac{\pi e^2}{m_e h\nu_{q,p}}\ f_{q,p}$$

The Einstein $\bar{A}$ and $\bar{B}$ coefficients can be related as follows.[11] Consider a Hohlraum where $dn/dt = 0$ for any energy level at any time, and where the radiation is Planckian. Then, equating transitions between p and q due to spontaneous and stimulated emission and absorption

$$\rho_R(\nu_{p,q})\ n(q)\ \bar{B}(q,p) = n(p)[\bar{A}(p,q) + \rho_R(\nu_{p,q})\ \bar{B}(p,q)]$$

Relating $n(q)$ to $n(p)$ by the Boltzmann expression, and realizing that $\rho_R(\nu_{q,p}) \equiv \rho_R(\nu_{p,q})$ the above equation reduces to,

$$\rho_R(\nu_{p,q}) = \frac{g(p)\ \bar{A}(p,q)}{\bar{B}(q,p)\ g(q)\ \exp(h\nu_{p,q}/kT) - g(p)\ \bar{B}(p,q)}$$

Comparing this relation with the Planckian form,

$$\rho_R(\nu_{p,q}) = \frac{8\pi h}{c^3}\ \nu_{p,q}^3 \left[\exp\left(\frac{h\nu_{p,q}}{kT}\right) - 1\right]^{-1}$$

results in the two Einstein relations,

$$g(p)\ \bar{B}(p,q) = g(q)\ \bar{B}(q,p)$$

and

$$\frac{\bar{A}(p,q)}{\bar{B}(p,q)} = \frac{8\pi h \nu_{p,q}^3}{c^3}$$

Finally, combining the expression between $\bar{B}(q,p)$ and $f_{q,p}$ with these Einstein relations enables the Einstein $\bar{A}$ coefficient to be represented by,

$$\bar{A}(p,q) = \frac{8\pi^2 e^2 \nu_{p,q}^2}{m_e c^3}\ \frac{g(q)}{g(p)}\ f_{q,p}$$

APPENDIX D

RELATION BETWEEN THE EXCITATION AND DE-EXCITATION RATE COEFFICIENTS

The excitation and de-excitation cross-sections for transitions between any two energy levels p and q of the atom depend only on the collisional energy, and can be derived by the method of detailed balancing in the following manner. Assume states p and q are in equilibrium with each other and with the free electrons, and that only collisional processes between electrons and atoms occur. Then the number of transitions from q to p due to such collisions will equal the number of transitions from p to q, and can be expressed as,

$$n_e\, n(q) \int f(\epsilon_q)\, \sigma(q \rightarrow p)\, d\epsilon_q = n_e\, n(p) \int f(\epsilon_p)\, \sigma(p \rightarrow q)\, d\epsilon_p$$

Here ϵ_p and ϵ_q are the energies of the colliding free electrons, with the atom in energy levels p and q respectively, and $\sigma(q \rightarrow p)$ represents the cross-section for transitions between levels p and q.

Now, the Boltzmann expression relates the number densities of atoms in states p and q as,

$$\frac{n(q)}{n(p)} = \frac{g(q)}{g(p)} \exp\left(\frac{E_{p,q}}{kT}\right)$$

and the Maxwellian distribution of electrons is denoted by,

$$f(\epsilon) = c(T)\ \epsilon\ \exp(-\frac{\epsilon}{kT})$$

where $c(T)$ represents a temperature dependent function. In addition, the energy balance dictates that,

$$E(q) + \epsilon_q = E(p) + \epsilon_p$$

where $E(p)$ and $E(q)$ represent the electronic energy of the atom in energy levels p and q respectively. Therefore, the previous relation equating the number of transitions between states p and q reduces to,

$$\frac{g(q)}{g(p)} \int c(T)\ \epsilon_q \exp\left(\frac{\epsilon_q - \epsilon_p}{kT}\right) \exp\left(-\frac{\epsilon_q}{kT}\right) \sigma(q \to p)\ d\epsilon_q$$

$$= \int c(T)\ \epsilon_p \exp\left(-\frac{\epsilon_p}{kT}\right) \sigma(p \to q)\ d\epsilon_p$$

This expression is satisfied if,

$$\sigma(p \to q) = \frac{\epsilon_q}{\epsilon_p}\ \frac{g(q)}{g(p)}\ \sigma(q \to p)$$

since $d\epsilon_q = d\epsilon_p$.

Because the resulting expression relates cross-sections which are atomic constants and therefore independent of temperature, it is valid even when the energy levels are not in thermal equilibrium.

The rate coefficient is defined as,

$$K(p,q) = \frac{1}{m_e} \int f(\epsilon_p)\ \sigma(p \rightarrow q)\ d\epsilon_p$$

Substituting into this expression a Maxwellian distribution for the electrons at temperature T_e, and the previously derived relation between the excitation and de-excitation cross-sections, results in,

$$\frac{g(p)}{g(q)} K(p,q) = \frac{1}{m_e} \int c(T_e)\ \epsilon_q\ \sigma(q \rightarrow p)\ \exp\left(-\frac{\epsilon_p}{kT_e}\right) d\epsilon_p$$

By using the previous energy balance and since $d\epsilon_q = d\epsilon_p$ the above relation becomes,

$$g(p)\ K(p,q) = g(q)\ K(q,p)\ \exp\left(-\frac{E_{q,p}}{kT_e}\right)$$

Summing over all of the excited levels $q > 0$ transforms the above expression to the following relation, for the case where p represents the ground state, 0, of degeneracy 1,

$$\sum_{q>0} K(0,q) = \sum_{q>0} g(q)\ K(q,0)\ \exp\left(-\frac{E_{q,0}}{kT_e}\right)$$

APPENDIX E

RATE OF ELECTRON PRODUCTION BY ATOM-ATOM IONIZING COLLISIONS

By following an analysis similar to that described in Chapman and Cowling[17] the rate of electron production due to inelastic encounters between atoms can be expressed as,

$$\left(\frac{dn_e}{dt}\right)_{A\text{-}A} = \frac{n_A^2}{4\pi^{1/2}} \left(\frac{m_A}{kT_A}\right)^{3/2} \int_{v_i}^{\infty} \exp\left(-\frac{m_A v^2}{4kT_A}\right) \sigma_{A\text{-}A}(v)\, v^3\, dv$$

where $\sigma_{A\text{-}A}(v)$ represents the ionizing cross-section for collisions between atoms, v is the relative velocity between each pair of colliding atoms and v_i is its value corresponding to the energy of the first excited level of the atom. Since the energy of such a pair of atoms relative to the axes moving with their center of mass is,

$$\epsilon = \frac{1}{4} m_A v^2$$

the above expression can be written in terms of ϵ as,

$$\left(\frac{dn_e}{dt}\right)_{A\text{-}A} = \frac{2n_A^2}{(m_A\pi)^{1/2}\,(kT_A)^{3/2}} \int_{\epsilon_i}^{\infty} \exp\left(-\frac{\epsilon}{kT_A}\right) \sigma_{A\text{-}A}(\epsilon)\, \epsilon\, d\epsilon$$

Assuming that the region of interest of the cross-section curve, i.e., that portion near the ionization threshold, can be

approximated by the following polynomial of degree n,

$$\sigma_{A\text{-}A}(\epsilon) = \sum_{m=1}^{n} c_m(\epsilon - \epsilon_i)^m$$

where ϵ_i is the energy of the first excited level of the atom, and the c_m's are constants, the electron production rate is,

$$\left(\frac{dn_e}{dt}\right)_{A\text{-}A} = \frac{2n_A^2 \exp(-\epsilon_i/kT_A)}{(m_A\pi)^{1/2}(kT_A)^{3/2}} \int_0^{\infty} \exp(-s/kT_A)(s + \epsilon_i) \sum_{m=1}^{n} c_m s^m \, ds$$

where $s \triangleq \epsilon - \epsilon_i$. Interchanging the integration and summation signs, the integrated expression becomes,

$$\left(\frac{dn_e}{dt}\right)_{A\text{-}A} = \frac{2n_A^2(kT_A)^{1/2}}{(m_A\pi)^{1/2}} \left[\sum_{m=1}^{n} c_m(m+1)!\,(kT_A)^m \left(\frac{\epsilon_i}{(m+1)kT_A} + 1\right)\right] \exp\left(-\frac{\epsilon_i}{kT_A}\right)$$

For a flowing gas the substantial derivative, for the electron production rate per unit mass of gas, must be used. In terms of this derivative the above expression becomes,

$$\frac{D}{Dt}\left(\frac{n_e}{\rho}\right)_{A\text{-}A} = \frac{2\rho(kT_A)^{1/2}}{(m_A)^{5/2}\pi^{1/2}} \left[\sum_{m=1}^{n} c_m(m+1)!(kT_A)^m \left(\frac{\epsilon_i}{(m+1)kT_A} + 1\right)\right]$$

$$\times \exp\left(-\frac{\epsilon_i}{kT_A}\right).$$

REFERENCES

[1]Petschek, H. and Byron, S., "Approach to Equilibrium Ionization Behind Strong Shock Waves in Argon," Annals of Physics 1, 270 (1957).

[2]Bond, J.W., "Structure of a Shock Front in Argon," The Physical Review 105, 1683 (1957).

[3]Harwell, K.E. and Jahn, R.G., "Initial Ionization Rates in Shock-Heated Argon, Krypton, and Xenon," The Physics of Fluids 7, 214 (1964).

[4]Wong, H., "Interferometric Study of Thermal Equilibration of a Shock Heated Plasma," Ph.D. Thesis, Stanford University, Stanford, Calif., (1964).

[5]Pomerantz, J., "The Influence of the Absorption of Radiation in Shock Tube Phenomena," J. Quant. Spectrosc. Radiat. Transfer 1, 185 (1961).

[6]Alpher, R.A. and White, D.R., "Optical Refractivity of High-Temperature Gases. I. Effects Resulting from Ionization of Monatomic Gases," The Physics of Fluids 2, 162 (1959).

[7]Horn, K.P., "Radiative Behavior of Shock Heated Argon Plasma Flows," SUDAAR No. 268, Stanford University, Stanford, Calif. (1966).

[8]Lagar'kov, A.N. and Yakubov, I.T., "The Effect of Radiation on the State of a Gas Ahead of a Shock-Wave Front," Opics and Spectroscopy 14, 103 (1963).

[9]Biberman, L.M. and Norman, G.E., "Plasma Radiation Due to Recombination and Bremsstrahlung Processes," J. Quant. Spectrosc. Radiat. Transfer 3, 221 (1963); General Atomic translation, GA-tr-4943 (1963).

[10]Bates, D.R., Kingston, A.E., and McWhirter, R.W.P., "Recombination Between Electrons and Atomic Ions. I. Optically Thin Plasmas," Proc. Roy. Soc. 267, 297 (1962).

[11]Nicholls, R. W., "Spectroscopic Methods of Gasdynamics," Lectures notes, Stanford University, Stanford, Calif. (1964).

[12]Knox, R.S., "Excited-State Wave Functions, Excitation Energies and Oscillator Strengths for Argon ($3p^5 4s$)," The Physical Review 110, 375 (1958).

[13]Olsen, H.N., "Measurement of Argon Transition Probabilities Using a Thermal Arc Plasma as a Radiation Source," J. Quant. Spectrosc. Radiat. Transfer 3, 59 (1963).

[14]Seaton, M.J., "Excitation and Ionization by Electron Impact," from Atomic and Molecular Processes, edited by D.R. Bates (Academic Press, Inc., New York, 1962), p. 416.

[15]Sluyters, Th.J.M., De Haas, E., and Kistemaker, J., "I. Charge Exchange, Ionization and Electron Loss Cross-Sections in the Energy Range 5 to 24 keV", Physica 25, 1376 (1959).

[16]Massey, H.S.W. and Burhop, E.H.S., Electronic and Ionic Impact Phenomena (Oxford University Press, London, England, 1952) p. 441.

[17]Chapman, S. and Cowling, T.G., The Mathematical Theory of Non-Uniform Gases, (Cambridge University Press, Cambridge, England, 1960), p. 90.

[18]Landau, L., "Die Kinetische Gleichung für den Fall Coulombscher Wechselwirkung," Physik. Z. Sowjetunion 10, 154 (1936).

[19]Longmire, C.L., Elementary Plasma Physics, (Interscience Publishers, New York, 1963), p. 167.

[20]Cambel, A.B., Duclos, D.P., and Anderson, T.P., Real Gases (Academic Press, New York, 1963), p. 68.

[21]de Voto, R.S., "Argon Plasma Transport Properties," SUDAER No. 217, Stanford University, Stanford, Calif. (1965).

[22]Rose, D.J. and Clark, M., Plasmas and Controlled Fusion, (MIT Press, Cambridge, Mass., 1961), p. 233.

[23]Vlases, G., Department of Aerospace Engineering Sciences, University of Colorado, Boulder, Colo., private communication 1966.

[24]Glass, I.I. and Kawada, H., "Prandtl-Meyer Flow of Dissociated and Ionized Gases," UTIA Report No. 85, University of Toronto, Toronto, Canada (1962).

[25]Liepmann, H.W. and Roshko, A., Elements of Gasdynamics, (John Wiley and Sons, Inc., New York, 1957), p. 59.

[26]Jaffrin, M.Y., "Shock Structure in a Partially Ionized Gas," Fluid Mechanics Laboratory Publication No. 64-9, Massachusetts Institute of Technology, Cambridge, Mass. (1964).

[27]Bates, D.R. and Damgaard, A., "The Calculation of the Absolute Strengths of Spectral Lines," Phil. Trans. Roy. Soc. London 242, 101 (1949).

[28]Conti, R.J., "A Theoretical Study of Nonequilibrium Blunt-Body Flows," Ph.D. Thesis, Stanford University, Stanford, Calif. (1964).

[29]Sibulkin, M., "Absorption and Emission Characteristics of an Ideal Radiating Gas," NONR 562 35/7, Brown University, Providence, R.I. (1965).

[30]Sevastyanenko, V.G. and Yakubov, I.T., "Radiation Cooling of a Gas Heated by a Powerful Shock Wave," Optics and Spectroscopy 16, 1 (1964).

[31]Delcroix, J.L., Introduction to the Theory of Ionized Gases, (Interscience Publishers, Inc., New York, 1960), p. 30.

[32]Unsöld, A., Physik der Sternatmosphären, (Springer-Verlag, Berlin, Germany, 1955), p. 278.